Summer 2012

Physiochemical characteristics contributing to the cytotoxicity of transition metal oxides

Chi-heng Wu

Department:

PHYSICOCHEMICAL CHRATERISTICS CONTRIBUTING TO THE CYTOTOXICITY OF TRANSITION METAL OXIDES

by

CHI-HENG WU

A THESIS

Presented to the Faculty of the Graduate School of the

MISSOURI UNIVERSITY OF SCIENCE AND TECHNOLOGY

In Partial Fulfillment of the Requirements for the Degree

MASTER OF SCIENCE IN APPLIED AND ENVIRONMENTAL BIOLOGY

2012

Approved by

Yue-Wern Huang, Advisor

Katie B. Shannon

Jeffrey G. Winiarz

ABSTRACT

In the past ten years nanotechonology has not only evolved to play a prominent role in our economy but also increased the concern over potential adverse effects caused by nanomaterials to human health and the environment. Nanotoxicity is to understand the nature and origin of the toxicity imposed by nanomaterials. Studies from our laboratory have shown that nanoparticle induces oxidative stress, perturbs calcium homeostasis, alter gene expression, and produces pro-inflammatory responses. We also identified a trend of toxicity: $TiO_2 < Cr_2O_3 < Fe_2O_3 < Mn_2O_3 < NiO < ZnO < CuO$. We then asked a question: what are physiochemical factors of transition metal nanoparticles that contributed to this increasing cytotoxicity.

In this thesis I investigated the correlation between physicochemical properties and toxicity of the transition metal oxides in the 4th Period of the Periodic Table of Elements. Particle size, BET surface area, point of zero charge, metal dissolution, and degree of surface adsorption of transition metal oxide nanoparticles were measured. There were no increasing trends in both particle size and specific surface area. The point of zero charge showed an increasing trend as $TiO_2 < Cr_2O_3 < Fe_2O_3 < NiO < CuO = ZnO < Mn_2O_3$. The number of available binding sites of nanoparticle showed an increasing trend as $Cr_2O_3 > ZnO > CuO > NiO > Fe_2O_3 > Mn_2O_3 > TiO_2$. The degree of adsorption on the surface of nanoparticles showed an increasing trend with atomic number, with the exception of Cr_2O_3. The degree of dissolution of transition metal oxides increases with atomic number. In summary, the factors that contribute to cytotoxicity of transition metal oxides were a combination of point of zero charge, number of available binding sites on the surface of nanoparticles, and metal dissolution. This study advances our understanding in mechanisms of nanotoxicity, which may lead to safer design of nanomaterials.

ACKNOWLEDGEMENTS

I would like to thank my advisor Dr. Yue-wern Huang for his support, guidance, and constant encouragement.

I appreciate Dr. Katie Shannon and Dr. Jeffrey Winiarz for serving as my committee members, and for their input.

I would like to thank Dr. Honglan Shi from the Department of Chemistry at Missouri University of Science & Technology for her technical support.

I am grateful for Dr. Daniel Forciniti of Department of Chemical & Biological Engineering at Missouri University of Science & Technology for use of research equipment.

I would like to thank Dr. Robert S. Aronstam from department of biology at Missouri University of Science & Technology for his support, collaboration, guidance, advice and comments.

I would like to thank Dr. Charles C. Chusuei of the Department of Chemistry at Middle Tennessee State University for his collaboration, guidance, advice, and comments on this research.

I greatly appreciated my friends Hsiu-Jen Wang, Ching Chang, Rhett Reichard, Adam Martin, Vanessa Kaighin, Li-Chieh Chou, Cheng-Ming Lin, Cheng-Ming Hsu, Jong-sik Moon, and Huei-Tong O Yang for their assistance and support. I am also grateful to receive help from the faculty members in the Department of Biological Sciences at Missouri University of Science and Technology. Finally, I would like to thank my parents, Kuo-Sen Wu and Shu-Chuan Chang, for their long-term encouragement and support of my graduate study. I want to thank my dear brother, Ho-Hsiang Wu, for his support and constant encouragement. Without their love and support, I could not have completed my graduate study in the U.S.A

TABLE OF CONTENTS

LIST OF FIGURES

Page

LIST OF TABLES

1. INTRODUCTION

1.1 OVERVIEW

Nanotechnology is the study of the control of matter on atomic and molecular scales. Nanomaterials are materials that have at least one dimension in the range of 1-100 nm [1]. Due to small sizes, they exhibit novel physical and chemical functional properties. Applications and production of new nanomaterials, especially metal oxides, are increasing in diverse fields [2], including cosmetic products [3], magnetocooling [4], optical and recording devices [5, 6], purification of enzymes and other biological materials [7], water purification devices [8], and biomedical research [9, 10]. Due to large production and demand, occupational workers and/or end product users may have exposure to nanomaterials via inhalation, dermal absorption, gastrointestinal tract absorption and injection of bioengineered nanomaterials. There is a growing concern that emerging nanotechonology may impose adverse effects to human health and the environment.

The Health Effect Institute (HEI), established in 1980, is an independent and unbiased source of information on the health effects of motor vehicle emissions, and has supported research on all major air pollutants. In 2000, the research report from HEI stated that ambient particulate matters with various sizes and chemical compositions contain very small particles (less than 100 nm in diameter) that are particularly toxic [11]. Yet, the research conducted by Oberdörster and colleagues conducted an inhalation study and found that ultrafine particles showed no greater adverse effects, including inflammatory response and pulmonary dysfunction. On the other hand, a sudy with instillation showed size-dependent toxicity between ultrafine particles and fine particles [12, 13]. The ultrafine particle was not discovered to cause the adverse effect on the animal model until instilling ultrafine particles directly into the trachea of animal.

Later on, the ultrafine particles (diameter <100 nm) and transition metal containing particulate air pollutants were found to cause the adverse effects *in vitro* and *in vivo* [14-16]. In 1999, Li and colleagues found that ultrafine carbon black (14 nm) possesses greater lung inflammation and oxidant stress than fine carbon black (250 nm). Moreover, Wilson and colleagues investigated interactions between ultrafine particles and transition metals [16]. The result showed that ultrafine carbon black (14 nm) reduced the levels of Glutathione (GSH) in J774 cells (murine macrophage cell line) while addition of iron salts ($FeCl_3$ and $FeSO_4$) to carbon black could further decrease GSH. This evidence suggested that the ambient particles with different size, chemical composition and surface characteristics could cause various adverse effects, such as oxidative stress and inflammatory response both *in vitro* and *in vivo*. According to these studies, it became suspicious that the nanoparticles which had similar characteristics as ultrafine ambient particles may have potentially adverse effects. In order to guide the future design of safe nanomaterials, identification and characterization such as size distribution, shape, and physical and chemical properties of nanoparticles will be critical to address potential effects on human health and environmental implications [17-20].

1.2 NANOTOXICOLOGY

Donaldson and his colleagues described framework of nanotoxicology to address potential threats in support of the growth of a safe and sustainable nanotechnology industry [21]. Nanotoxicology encompasses physicochemical characterization, routes of exposure, biodistribution, molecular markers, genotoxicity, neurotoxicology, etc. While *in vivo* studies investigate health effects, *in vitro* studies can elucidate mechanisms of toxicity without influence of toxicokinetics and toxicodynamics.

In our laboratory, we have investigated cytotoxicity, oxidative stress, perturbation of membrane integrity, alteration of gene expression, and imbalance of calcium homeostasis in human lung cells, both BEAS-2B and A549 [22]. Nanoparticles could cause dose-dependent and time-dependent effects on cytotoxicity. Also, the integrity of the cell membrane was compromised by measuring the LDH leakage, the oxidative stress was induced by measuring the reactive species, and oxidative-related gene expression was altered using pathway-specific DNA microarray. One missing piece of information is what factors contribute to the adverse effects.

1.3 CYTOXICITY OF TRANSITION METAL OXIDES

Cytotoxicity of nanoparticles could be cell line dependent [23]. For instance, Syed and colleagues showed that nanoparticles such as TiO_2, SiO_2, MWNT, and MWCNT caused differential toxicity in 3T3 (fibroblast), hT (telomerase-immortalized human bronchiolar epithelial cells), and RAW 264.7 (murine macrophage) cell lines. Aside from differences in cell lines, toxicity of transition metal nanoparticles could be particle species-dependent [24-27]. For instance, TiO_2 was known to be less toxic than CuO and ZnO in zebra fish [28], soil nematode [29], human cell lines (HEp-2 and keratinocytes) [30, 31], and marine species [18]. For instance, ZnO nanoparticles had smaller LC50 value than TiO_2 on nematode *Caenorhabditis elegans*. These studies indicated particle specific effects. Recently our laboratory identified a trend of toxicity of transition metal oxides of TiO_2, Cr_2O_3, Fe_2O_3, Mn_2O_3, NiO, CuO, and ZnO: as atomic number increases, toxicity increases and we summarized an nanoparticle-induced cell death in Figure 1.1 [32]. Synergistic interactions between intracellular [Ca^{2+}] and oxygen species were potential factors which lead to cell death. As intracellular [Ca^{2+}] and oxygen species could affect each other, they both could induce cell programmed death (apoptosis) by distinct pathways. While we have identified several inter-related cellular responses to nanoparticle exposure, it remains unclear what physicochemical properties of nanoparticles govern cytotoxicity.

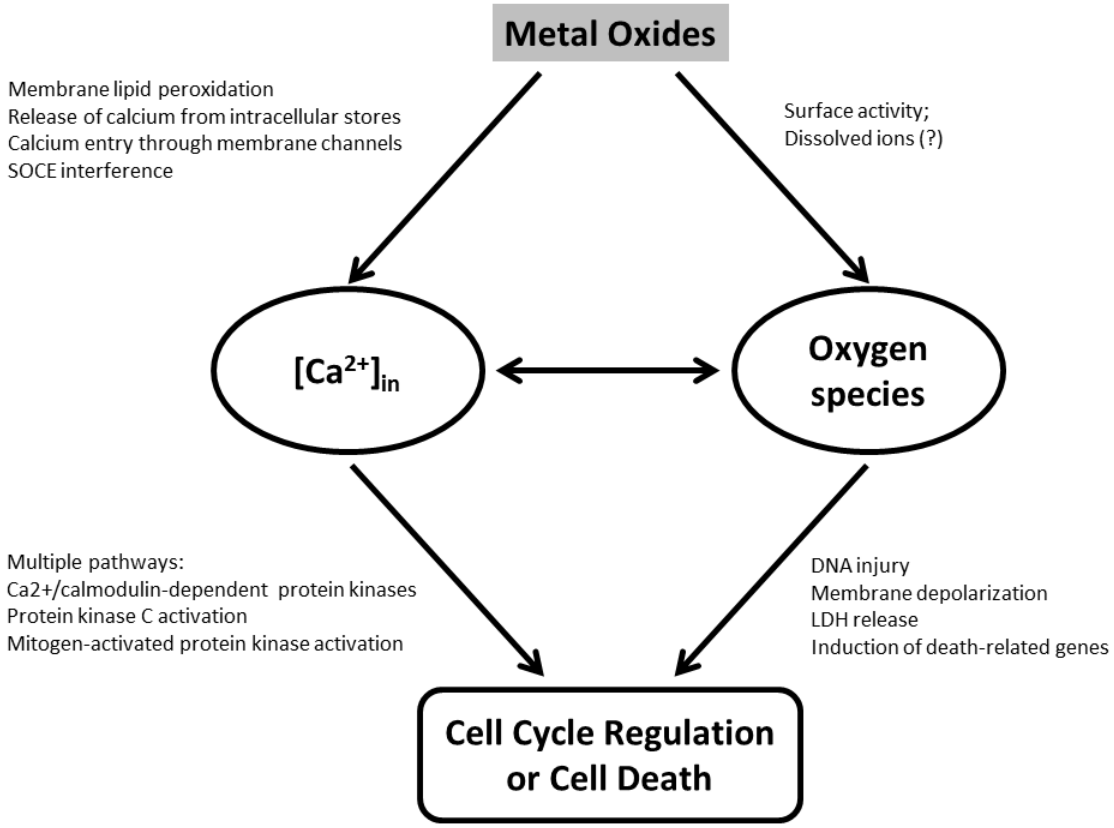

Figure 1.1: Cell death induced by nanoparticle. The figure shows the relationships between nanoparticles, production of reactive oxygen species, and intracellular Ca2+ concentrations. (from [32])

1.4 CHARACTERIZATION OF NANOPARTICLES

Characterization of nanoparticles is essential in nanotoxicity studies as particle's properties may influence toxic outcome. Due to the unique characteristics of nanoparticles, such as small size (<100 nm) and corresponding large specific surface area (SSA), nanoparticles were thought to impose higher degrees of biological effects as cytotoxicity, oxidative stress, metabolism and homeostasis than their corresponding micro-sized particles [33-36]. Assuming equal particle mass, as particle sizes decrease, surface areas increased dramatically. Nanoparticles may possess higher bioreactivity per given mass when compared to micro-scaled particles. The property can be utilized for biomedical applications such as contrast-enhanced MRI agent [37-39], molecular image [37, 40, 41], and drug delivery [42-44]. On the other hand, increased SSA may impose higher oxidative stress [4, 5, 25, 45-47], immune response [48-50], damage of intracellular molecules (e.g., DNA, proteins) [8, 47, 51, 52], and cell death. Additional reports showed that nano-sized metal oxides were more toxic than their corresponding macro-sized one *in vitro* and *in vivo* [29, 53-55]. For instance, two sizes of CuO nanoparticles (20~40 nm and 3000 nm) were treated in human alveolar type II-like epithelial cell line (A549) for 18 hr. Nano-size CuO caused greater cytotoxicity than micro- size one at same concentration [55].

The physicochemical characterizations such as point of zero charge (PZC), and particle surface binding sites may also play a role in cytotoxicity. Point of zero charge describes a condition when electrical charge density on a surface is neutral. Based on the electrical double layer model and the Gouy-Chapman theory [56, 57], the PZC could be elucidated more clearly. A double layer is a structure that appears on the surface of a solid particle or a liquid droplet when exposed in an aqueous environment. The particles are surrounded by two layers of charge in an aqueous environment, (Figure 1.2**)**. The First layer consists of adsorbed ions on the surface of particles. The second layer is called diffuse layer as it is loosely bound with the object rather than being firmly

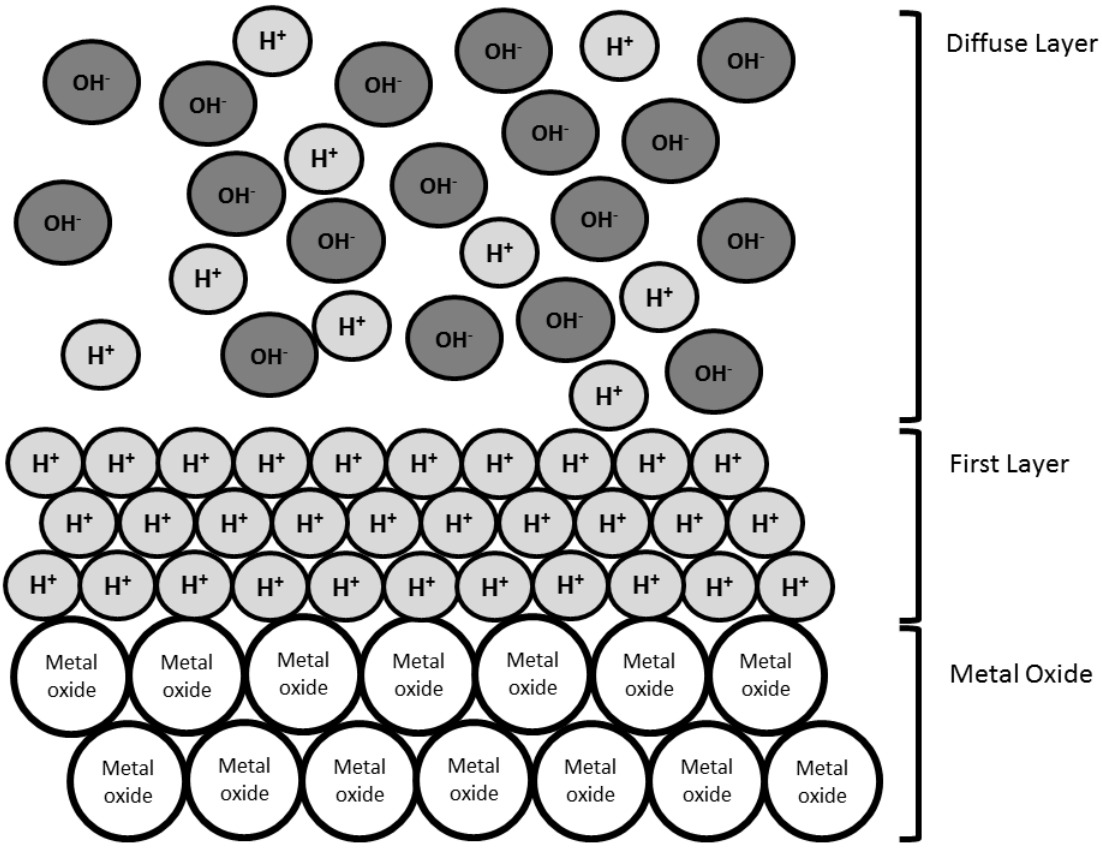

Figure 1.2: The double layer theory.

anchored. The net electrical charge in the diffuse layer is equal in magnitude to the net surface charge, but with opposite polarity, hence making the entire structure electrically neutral. As the pH of the solution was equal to the PZC, the net charge of the surface was zero. The net charge of surface is positive as the pH of the solution is below the PZC because the proton would be adsorbed by nanoparticles. When the pH of the solution is above PZC, the net charge will be negative. The PZC of transition metal oxide is critical because it indicates the adsorption of ions and biological molecules. Once the PZC is determined, we can predict the charge associated with molecules which would be adsorbed by nanoparticles. The PZC measurements were carried out according to the method developed by J. Park and J.R. Regalbuto [58] and modified for use to measure PZC of nanomaterials in our laboratory.

X-ray photoelectron spectroscopy was a quantitative spectroscopic technique to study the energy distribution of the electrons emitted from X-ray-irradiated materials [59]. The simplified instrumental setup was showed in Figure 1.3. The photoelectric effect, the basic concept of XPS, is a phenomenon in which electrons are ejected from a surface, when photons of adequate wavelength are incident. The electrons which absorb the energy from the photons with no loss of energy would eject from the surface of materials and exhibit the excess energy which would be converted into kinetic energy of electron. The measurement of kinetic energy of the escaped electron provided information for its initial atomic and molecular states. According to the article [59], the chemical shift of an atom shown that the electron binding energy was a function of the chemical environment of the atom. For instance, the spectrum of the carbon 1s level in ethyl- trifluoroacetate ($CF_3COOC_2H_5$) had four peaks present -CF_3, -COO, -CH_2, -CH_3, and these large chemical shifts in the carbon 1s level, due to different surrounding atoms, indicated the power of the XPS method in Figure 1.4.

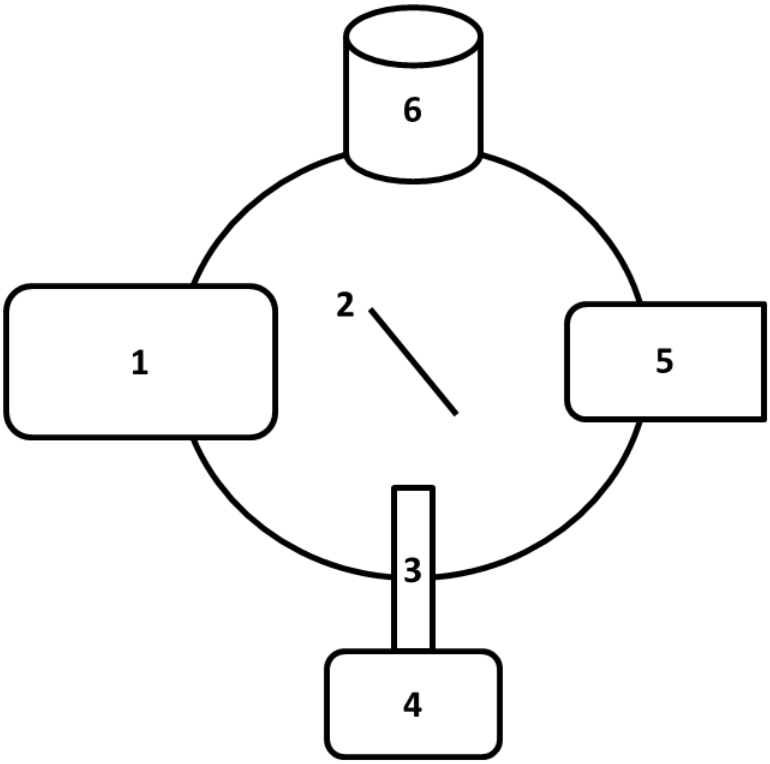

Figure 1.3: XPS instrumental setup 1.) The entry and exit of samples into the chamber took place through a series of sliding seals and gate valves. 2.) This was the ultra high vacuum chamber, where pressure in the order of 10-8 to 10-10 Torr . 3.) X-ray gun. 4.) X-ray source, which produced monochromatic X-rays. 5.) Double pass cylindrical analyzer, which analyzed the incoming photoelectrons. 6.) The turbo pump and roughing pumps were used to water cool the heat.

`

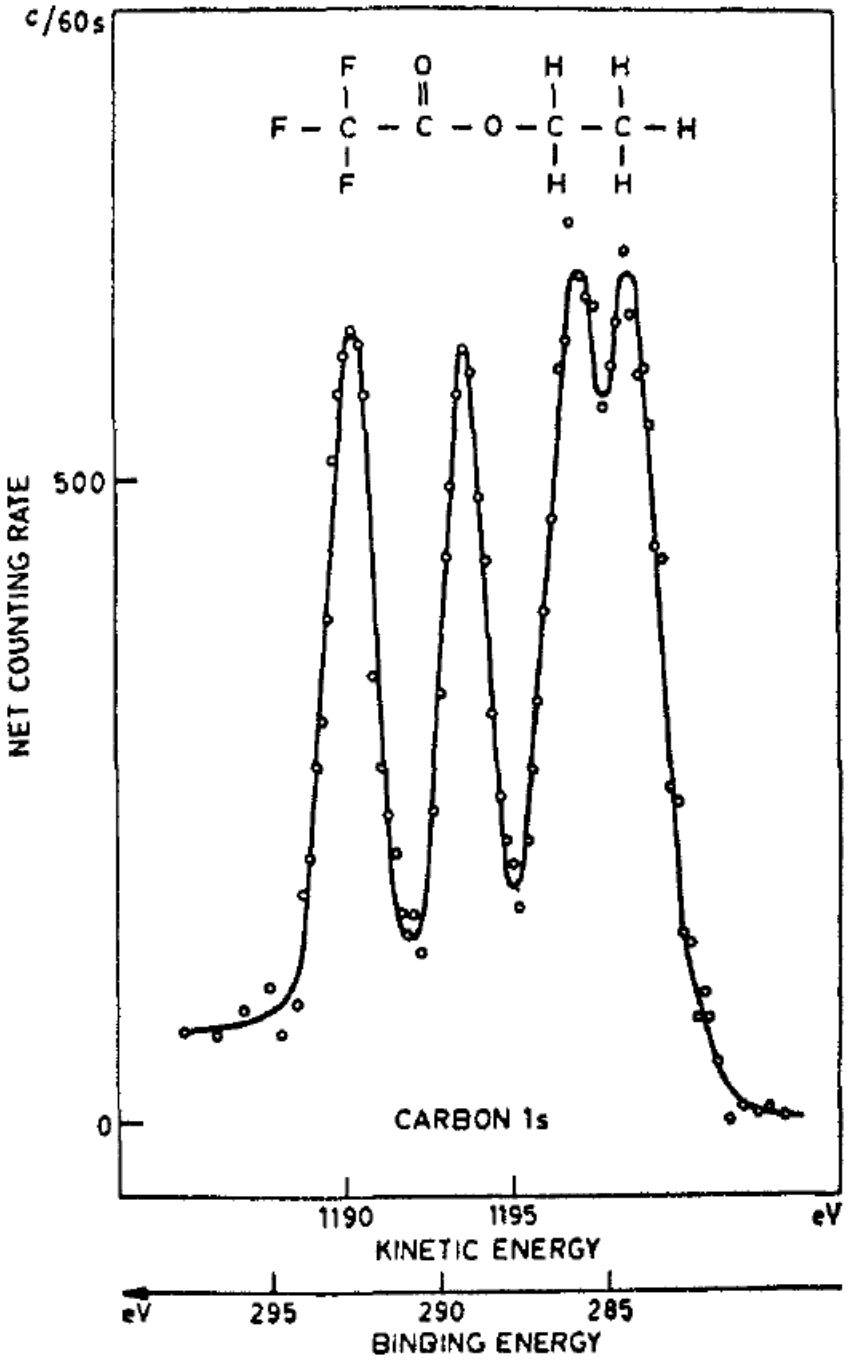

Figure 1.4: Carbon 1s photoelectron spectrum of ethyl trifluoroacetate (figure adapted from K. Siegbahn et al. ESCA; Atomic, Molecular and Solid State Structure Studied by Means of Electron Spectroscopy. Ser. IV, volume 20, 1967).

1.5 METAL ION RELEASED FROM TRANSITION METAL OXIDES

In addition to the above-mentioned properties of nanoparticles, metals from oxide compounds may dissolve in aqueous environment. Studies have shown metal ions can cause toxicity *in vitro* and *in vivo* [15, 60, 61]. For instance, Martin R. Wilson and colleague demonstrated that metal ions adsorbed on carbon blacks are the main culprit of toxicity that included alteration of morphology, cell death, and inflammation [15]. Moreover, Xia and colleagues investigated toxicity caused by dissolution of ZnO and CeO. They concluded that dissolution of ZnO plays a critical role in contributing cytotoxicity [61]. The potential role of dissolved ions in toxicity was also highlighted in a study by George *et al.* [62]. In 2010, George et al. demonstrated that 1) cytotoxicity of ZnO was significantly reduced by doping ZnO with iron, and 2) the pure and decreased levels of Fe-doped ZnO nanoparticles released remarkably high levels of Zn^{2+} into aqueous solutions. The iron was proposed to stabilize the crystal structure of ZnO and thus decreased dissolution of ZnO. Moreover, Beck-Spider et al. showed that the adverse effect, such as increased neutrophil influx and cytokine (IL-6), was caused by soluble metal ions [60].

To measure degree of metal dissolution from metal oxides, particles were weighed and placed in an aqueous solution for a designated period of time. The sample was then centrifuged at 120,000 rpm for at least 5-30 min to separate nanoparticles from metal ions. The supernatant containing metal ions is then analyzed using an inductively coupled plasma mass spectrometry (ICP-MS) and graphite furnace atomic absorption spectrometry (GFAAS). The pH of the solution may not be constant during the experiments and the ultracentrifugation could not completely pull down nanoparticles. In this study, we have developed a method that takes these issues into account.

Studies have shown that nanoparticles are internalized into cells via endocytosis and trapped in lysosome. The particles may be released from lysosome into cytosol at certain point in time. It is unclear whether there are differential degree of metal dissolution from metal oxides between cytosol and acidic lysosome. In this study, we

simulate the pH of cytosol and lysosome (7.4 and 4.5, respectively) to investigate the metal dissolution. According to our pilot studies, we found that the nanoparticle could alter the pH of the solution to which it was exposed. Hence, we employed autotitration to maintain the pH condition. Moreover, we noticed that metal oxide nanoparticles could not be completely pulled down by ultracentrifugation, and the nanoparticle pellets could be easily disturbed during pipetting. Hence, we employed a dialysis membrane to separate oxide nanoparticles from metal ions. We then transferred samples into a dialysis membrane to allow for reaching equilibrium. The samples were finally analyzed by ICP-MS and GFAAS.

1.6 INDUCTIVELY COUPLED PLASMA MASS SPECTROSCOPY

Inductively coupled plasma mass spectrometry (ICP-MS) is an analytical technique used for the qualitative and quantitative determination of elements in solution or liquid samples. ICP-MS was developed in the late 1980's to combine the easy sample introduction and fast analysis of ICP (Inductively Coupled Plasma) technology with the accurate and low detection limits of a mass spectrometer. The instrument is capable of tracing multi-element analysis, often at the part per trillion levels. An ICP-MS combines a high-temperature ICP source with a mass spectrometer. In general, the argon gas was heated and formed a plasma flame, and the plasma flame would convert the atoms of the elements in the sample to ions. These ions were then separated and detected by the mass spectrometer. The ion concentration of the samples can be determined through calibration with multi-element reference standards.

1.7 GRAPHITE FURNACE ATOMIC ABSORPTION SPECTROMETRY

Graphite furnace atomic absorption spectrometry (GFAAS) is now considered one of the most reliable methods of measuring quantities of trace elements, and a type of spectrometry that is equipped with a graphite-coated furnace to vaporize solid and aqueous samples. The basic concept of GFFAS is based on the fact that ground-state atoms are capable of absorbing energy, such as light, and the amount of the absorbance is linearly correlated to the concentration of analyte. Generally, a matrix modifier is added to the sample prior to heating so that the chemical form of the analyte is controlled during the heating sequence. Samples are deposited in a graphite tube, which can produce 3,000^{o}C to vaporize and atomize the analyte. After the samples were atomized, the ground-state atoms will absorb ultraviolet light and transition to higher electronic energy levels. The absorbance would be recorded by spectrometry. Concentration measurements are determined by calibrating the instrument with reference standards.

1.8 RESEARCH OBJECTIVE

Accordingly, our research aims are

1. Cytotoxicity of transition metal oxides in BEAS-2B and A549
2. Physicochemical properties contributed to cytotoxicity
    a. Characterization of transition metal oxides including size, SSA and morphology
    b. Point of zero charge indicates the net charge on nanoparticle surface in aqueous environment
    c. The number of available binding sites on nanoparticle surface
    d. Metal dissolution of transition metal oxides
3. Analyze the correlation among physicochemical properties and cytotoxicity using spearman's rank correlation coefficient

An increasing trend in cytotoxicity of 4^{th} period transition metal oxide nanoparticles was observed in our lab [32] and the physicochemical factors which contributed to cytotoxicity were not clearly defined. The goal of my study was to investigate the various physicochemical properties of transition metal oxide nanoparticles: TiO_2, Cr_2O_3, Mn_2O_3, Fe_2O_3, NiO, CuO and ZnO, and explore possible correlations between the physicochemical properties and cytotoxicity. The cytotoxicity of the transition metal oxides were measured using SRB assay on two cell lines regarded as A549 and BEAS-2B. The physicochemical properties such as particles size, specific surface area, point of zero charge, number of available surface binding sites, and dissolution were studied by various methodologies developed in our lab according to previous research. Transmission electron microscopy and ImageJ software would be used to identify the shape and size distribution of nanoparticles. Specific surface area measurements were measured by BET method. The available sorption on surface area of metal oxide would be quantified by XPS. PZC measurement was done based on the method designed by Park and Regalbuto [58]. The dissolution studies of transition metal oxide nanoparticles which were added into 0.01 M NaCl solution was measured at two

constant physiological conditions (pH4.5 and 7.4) and for time points of 6, 12, 18 and 24 hr. This study was undertaken to delineate the various physicochemical properties of metal oxide nanoparticles which influence their cytotoxicity.

2. MATERIALS AND METHODS

2.1 CHEMICAL AND MATERIALS

Transition metal oxide nanoparticles, TiO_2, Cr_2O_3, Mn_2O_3, NiO, CuO, and ZnO, were purchased from Nano structured and Amorphous Materials (99.9% purity; Los Alamos, New Mexico, USA) and stored in a cabinet supplemented with nitrogen gas to avoid moisture and oxygen. For sample preparation, dried nanoparticles were incubated at 100^{o}C overnight to get rid of moisture, and then weighed in a sample vial using six digit analytical balances. The sample vials containing nanoparticles were stored in a cabinet supplemented with nitrogen gas for further usage, and could be stored no longer than 1 week.

The human bronchoalveolar carcinomaderived cell line (A549) and immortalized human bronchial epithelial cells (BEAS-2B) were purchased from ATCC (Manassas, VA, USA). These continuously cultured cells are widely used as an *in vitro* model for studying the prevention of the development of human lung carcinomas, as well as for nanotoxicity tests [63, 64]. The culture medium for BEAS-2B contained 500 ml Bronchial epithelial cell basal medium (Lonza, USA), 0.5 ng/mL recombinant epidermal growth factor (EGF), 500 ng/mL hydrocortisone, 0.005 mg/mL insulin, 0.035 mg/mL bovine pituitary extract, 500 nM ethanolamine, 500 nM phosphoethanolamine, 0.01 mg/mL transferrin, 6.5 ng/mL 3,30,5-triiodothyronine, 500 ng/mL epinephrine, 0.1 ng/mL retinoic acid, trace elements (Cambrex, USA), and 5 mL of 10,000 unit/mL penicillin plus 10,000 µg/mL streptomycin (MP, USA). The culture medium for A549 contained 445 mL Ham's F-12 medium (Cellgro, USA) supplemented with 50 mL fetal bovine serum (Thermo, USA), and 100,000 units/mL penicillin and 100,000 μg/mL streptomycin (MP, USA). Phosphate buffer saline (PBS) was prepared with 8 g NaCl, 0.2 g KCl, 1.44 g Na_2HPO_4, and 0.24 g KH_2PO_4 in 1 mL ddH_2O, autoclaved, and stored at 4^{o}C. Trypsin-EDTA was diluted from 10X Trypsin (Nalgene, USA) in PBS and added EDTA with a final concentration at 0.53 mM.

2.2 CELLS AND TREATMENT WITH NANOPARTICLES

Cells were grown at 37^{o}C in an incubator with a 5% CO_2 humidified environment. For cytotoxicity assay and pH change in medium assay, 100,000 cells were seeded into each well of a 24-well plate, and allowed to attach and grow for 24 hr at 80% confluence before any further treatment. The nanoparticles suspension was prepared freshly before each experiment. The appropriate amount of cell culture medium was added into sample vials containing nanoparticles to make 1 mg/mL stock nanoparticles suspension. The sample vials were sealed with parafilm and then sonicated for 15 min. The stock suspension was used to achieve various concentrations by series dilution and then the treatment was immediately applied to cells to minimize agglomeration. Cells not treated with nanoparticles served as a control group.

2.3 CYTOTOXICITY OF TRANSITION METAL OXIDES IN BEAS-2B AND A549 CELLS

In 1990, Skehan and colleagues had developed a methodology, called Sulforhodamine B ($C_{27}H_{30}N_2O_7S_2$, abbreviated as SRB) colorimetric assay, for large *in vitro* anticancer-drug-screening [65, 66]. The mechanism of SRB was based on its pH dependent ability to bind electrostatically on protein basic amino acid residues of trichloroacetic acid-fixed cells. It would bind to the amino acid under acidic circumstances and dissociate at basic conditions. The cell proliferation data testing with more than 25 compounds by SRB assay was nearly identical when compared with the data obtained by metabolic reduction of 3-(4,5-dimethylthiazol-2-yl)-2,5-diphenyltetrazolium bromide (MTT) assay [66]. We decided to employ the SRB colorimetric assay to measure the cell proliferation rather than MTT or MTS assay because it had been reported that the superoxide or oxygen reactive species could compromised the cell viability data from MTS and MTT assay [67]. From this evidence, we chose the SRB assay to test the cytotoxicity of our transition metal oxides.

To determine the cytotoxicity of seven transition metal oxides, BEAS-2B and A549 were treated with series concentration of metal oxides. Untreated cells served as

a control group. After 24 hr treatment, the cells were fixed with trichloroacetic acid for 1 hr in 4^{o}C refrigerate. The cells were washed with ddH_2O for 3 times and allowed to dry out completely. The cells were stained with 0.2% SRB in 1% acetic acid for 30 min. 0.2% SRB in 1% acetic acid was discard, and then the cells were washed with 1% acetic acid for 20 min, 3 times. The cells were incubated with 10 mM tris base for 20 min in room temperature. The 10 mM tris base was then transferred into a clean 96 well plates. The absorbance (510 nm) was determined by FLUOstar OMEGA (BMG LabeTech, USA).

2.4 PARTICLE SIZE MEASUREMENTS ON TRANSITION METAL OXIDE PARTICLES

Particle morphology and size were characterized using transmission electron microscopy (TEM) with a JEOL 1400 instrument operated at 120kV. Approximately 1 mg of each nanoparticle was placed in 1 mL of doubly distilled deionized water in an Eppendorf tube, sonicated and microliter aliquots were applied to 400-mesh carbon-coated copper grids (Electron Microscopy Sciences) and allowed to dry in N_2 atmosphere prior to microscopy. TEM images were saved in TIFF file format and examined using ImageJ ver. 1.44 software (National Institutes of Health, Gaithersburg, MD) to measure individual particle sizes and generate resulting histograms. The diameter of single nanoparticle was measured. The size of nanoparticle with spherical shape was determined by diameter. The size of nanoparticle with rod shape was determined according to their total length. The particle size measurements of seven transition metal oxides were imported to Microsoft Excel and a size distribution table for each metal oxide was generated with various increments of diameter and frequency. A differentiation size distribution histogram was generated with $\log_{10}$-transformed size of the nanoparticles on the X-axis and frequency divided by the $\log_{10}$-transformed increments of size. The frequency is adjusted by the increments to give a relative frequency. This relative frequency indicated that the amount of nanoparticle at specific diameter. The fitted line was added according to the student's t-distribution with n-1 degrees of freedom. The student's t-distribution used the sample standard deviation

instead of population standard deviation to estimate a normal distribution. This allowed us to construct a confidence interval that depends on estimable components.

2.5 BET SURFACE AREA MEASUREMENT ON TRANSITION METAL OXIDE PARTICLES

The specific surface area (surface are/unit mass) characterization of the nanoparticles generally followed the BET method [68]. In 1938, Stephan Brunauer, Paul Hugh Emment, and Edward Teller postulated the BET theory. BET theory illustrated that the physical adsorption of gas molecules on a solid surface, and the calculation of surface area and specific surface area of solids. Moreover, the gas molecules were physically adsorbed on solid layers and had no interaction between each adsorption layer. This methodology gave an idea of the physicochemical reactivity of nanoparticles. In this study, the specific surface area measurements of all the transitional metal oxide nanoparticles were made by Quantachrome Autosorb 1-C instrument using N_2 as the probe molecule. The instrument was fully automated and the samples were outgassed to expel moisture and weighed to determine dry mass of the nanoparticles. Seventy-eight data point complete gas adsorption isotherms were used to determine the specific surface areas.

2.6 POINT OF ZERO CHARGE MEASUREMENT ON TRANSITION METAL OXIDE PARTICLES

40 mL aliquots of pure water with various pH values ranging from 1 to 13 were prepared by adding HNO_3 and NaOH, and nanoparticles which were dried in 100 ^{o}C oven overnight. 13 external thread cryogenic vials were labeled from pH 1 to pH 13 and then weighed 10 mg nanoparticles in each vial by 6 digits analytical balance. The 10 mg of nanoparticles is determined based on the pilot studies conducted in our lab. Moreover, the 2 and 4 mg of nanoparticles would disappear in extreme pH valued aqueous solutions, i.e. pH 1-4 and 11-13, and then became a transparent solution. After the

amount of nanoparticles was increased to 10 mg, nanoparticles could be seen at the bottom of vial. This might indicate that the nanoparticles would be eroded or dissolved in the extreme pH environment. Cautiously, an aliquot of 1.8 mL of pH 1 water was added into the first cryogenic vial, pH 2 water into the 2nd one, and then pH 3 pure water into 3rd one, etc. The vials were set on a table without violent vibration in room temperature for 16 hr. After 16 hr, the pH in the interphase between surface of nanoparticles and supernatant of solution is detected by the spear-tip combination pH probe (Cole Parmer, catalog number G-05988-20). A graph was plotted with initial pH of each vial on the x-axis and the final pH in the interphase on the y- axis. The PZC value was obtained from the curve. The pH at which there was plateau in the line was the PZC value of the transitional metal oxide particles.

2.7 X-RAY PHOTOELECTRON SPECTROSCOPY (XPS) ON TRANSITION METAL OXIDE PARTCILES

The transition metal oxide nanoparticles (TiO_2, Cr_2O_3, Mn_2O_3, Fe_2O_3, NiO, CuO and ZnO) were reacted in a constant composition reactor, imitating the physiological conditions of pH 7.4. Metal oxide nanoparticles were dried in an oven overnight and weighed to 125.00 mg. The nanoparticles were dissolved in 25 mL of 0.01 M NaCl aqueous solution in a Nalgene plastic beaker. The 702 SM TiTRINO, METROHM AG CH-9101 (Herisau, Switzerland) was employed to monitor the pH of the solution. The pH of the solution was maintained at 7.4 for 16 hr duration by adding HCl (0.05 M). After 16 hr of constant composition at pH 7.4, the nanoparticle solution was filtered on to a 45 µm size Teflon filter paper (MicronSep). The filter paper was allowed to dry completely. The dried filter paper with nanoparticles was cut into small square pieces, which were then mounted onto clean tantalum foil using double sided tape. The edges were trimmed as required. All the equipment required for sample preparation such as scissors and tweezers were sonicated with acetone for 5 min before use, to prevent contamination. All of the sample preparation had been employed for all the metal oxide nanoparticles.

The number of available binding sites of each metal oxide sample were quantified using a Kratos Axis 25 X-ray photoelectron spectrometer integrated peak area ratios of physisorbed-to-metal oxide oxygen, monitoring the O 1s orbital after a 16-hr constant composition (CC) reactions maintaining solution conditions at pH = 7.4. XPS used a beam of X-rays to irradiate the sample, and simultaneously measured the kinetic energy and number of electrons that escape the surface. Ultra high vacuum condition (10^{-8} to 10^{-10} Torr) are required for running the XPS experiments to avoid scattering of photoelectrons ejected from the sample, travelling towards the detector. The XPS data were curved fitted using CasaXPS VAMAS software version 2.2 (Devon, UK).

2.8 METAL DISSOLUTION OF TRNASITION METAL OXIDE PARTICLES

The transitional metal oxide nanoparticles were added into 0.01 M NaCl solution with pH 4.5 and 7.4, respectively, while maintaining the pH value with the 702 SM TITRINO. The 0.01 M pH 7.4 NaCl solutions were used to imitate the pH value of cytosol environment, and the 0.01M pH 4.5 NaCl solutions were used to mimic the pH value of lysosome. The 702 SM TITRINO was employed to maintain the constant pH value as 4.5 and 7.4, respectively.

Reagents

- Pure water
- NaOH: trace metal grade
- Stock HCl: trace metal grade
- HNO_3: trace metal grade
- Centrifuge tubes
- Beaker
- Class B glass vials
- Dialysis membrane

Preparation of working solution and equipment

1. 0.001 M NaCl: Dissolved 0.292 g NaCl in 400 mL pure H_2O and then adjust pH to 4.5 or 7.2 using NaOH and HCl. Make up to 500 mL with pure H_2O. Store at 4^oC.
2. 3% HNO_3: Add 30 mL HNO_3 to 900 mL pure H_2O and then make up to 1 L with pure H_2O. Store at room temperature.

3. 1% HCl: Added 10 mL of stock HCl into 900 mL pure H_2O and then made up to 1 L with pure H_2O. Store at room temperature
4. 5% HCl: Added 50 mL HCl stock into 900 mL pure H_2O and then made up to 1 L with pure H_2O. Store at room temperature
5. Beakers, centrifuge tubes, glass vials, closures, stir bars, forceps, and scissors were acid wash with 3% HNO_3 overnight. The caps of centrifuge tubes and glass vials, and the plastic closure were acid washed for 15 min since these items could not resist strong acid for a long time. After the acid wash, all instruments were rinsed with pure water to remove the acid. And the equipment was air-dried inside a chemical hood to avoid any dust attaching on it.
6. Nanoparticles were dried in 100 ^{o}C oven overnight.
7. Gloves were worn during experimental operations to avoid contamination with organic residue.

Procedures

1. Weighed 250 mg nanoparticles in sample vials and then stored in chemical cabinet supplemented with nitrogen gas to avoid oxygen and moisture.
2. Gently, transferred 250 mg nanoparticles from sample vials into 200 mL beaker and then rinsed the vials with 50mL 0.001 M NaCl solution to completely transfer the nanoparticles into the beaker.
3. Forceps were used to move stir bars into the beaker and then opened the auto-titration machine.
4. Recorded the initial pH.
5. Adjusted pH value to 4.5 or 7.4 by HCl or NaOH, and recorded the volume of HCl and NaOH usage.
6. 702 SM TITRINO was then employed to mimic the constant pH value of 4.5 and 7.4, respectively.
7. At each time point, 6, 12, 18 and 24 hr, the pH and the volume of HCl and NaOH usage were recorded, and then a serological pipette was used to transfer 4 mL of

solution from the beaker into a centrifuge tube. Store centrifuge tube at 4^{o}C before further usage.

8. After collecting samples at 4 time points, centrifuged samples at 4^{o}C, 12,000 rpm for 5 min.
9. Measured the mass of empty glass vials and then added 25 mL pure water into glass vials.
10. Measured the mass of water-contained glass vials.
11. Serological pipette was used to transfer a 2 mL sample from the centrifuge tube into a dialysis membrane and then sealed the membrane by plastic closures.
12. Transfer another 1 mL sample into a small glass vial and then acidified with stock HCl. Store at 4^{o}C for further analysis.
13. Transferred the dialysis bag into 25 mL water-contained glass vials and then measured the weight of whole glass vials.
14. Put the glass vials on a shaker for 17 hr. The metal oxide would remain inside the dialysis bag while the metal ion which was released from metal oxide could diffuse through the dialysis membrane.
15. After 17 hr, removed the dialysis bag with caution by forceps. Did not let the forceps contact or merge into the pure water in order to avoid any contamination.
16. Weighed the glass vials, and then compared the record of weight in order to identify any leakage from dialysis membrane which may have happened.
17. Acidified the sample with stock HCl for long time storage to avoid the adsorption of metal ions. Stored samples at 4^{o}C for further analysis.

2.9 ANALYSIS OF METAL DISSOLUTION OF METAL OXIDE NANOPARTICLES BY ICP-MS AND GFFAS

Dissolved metal elements, Ti^{4+}, Cr^{3+}, Mn^{3+}, Ni^{2+}, Cu^{2+}, and Zn^{2+} were detected using an Elan-DRCe ICP-MS (Perkin-Elmer) equipped with a cyclonic spray chamber, a Meinhard nebulizer, platinum cones, and a CETAC ASX-500/ADX-100 autosampler. The ICP-MS analysis conditions were as follow: RF power was 1,300 W, argon flow rates for

the plasma and auxiliary gas were 15 and 1.2 L/min, respectively, and samples were delivered at 1.0 ml/min by a peristaltic pump. Internal standards were added continuously online as a mixture. Fe was determined with a graphite furnace atomic absorption (GFAA) method. An Analyst 600 atomic absorption spectrometer (PerkinElmer) was used. The ICP-MS operational conditions were summarized in (Table 2.1**)**.

Table 2.1: ICP-MS operational conditions

Parameter	Operation setting
ICP RF power	1300
Plasma gas flow	15 L/min
Auxiliary Gas	1.2 L/min
Nebulizer gas flow	0.99 L/min
Sample introduction system	Cyclonic spray chamber with meinhard nebulizer
Detector mode	Single
Auto Lens	Enabled
Lens voltage	6.5 V
Analog stage voltage	-1600 V
Pulse stage voltage	850 V
Sampler cone	Platinum, 1.1 mm orifice
Skimmer cone	Platinum, 0.9 mm orifice
Mass resolution	0.7 amu
Operating vacuum pressure	6.2 x 10-6 torr

To ensure the good quality data, most of the QA/QC those recommended by the EPA methods were followed. Instrument responses were calibrated with standard solutions using a range of concentrations. The detection limits were calculated at signal/noise ratio 3 to 5. The linear ranges of the calibration were determined and used for the quantitative analysis of the samples. Good linearity (R^2 = 0.9999 - 1) were obtained (Figure 2.1). The detection limits of Cu, Cr, Mn, Ni, Ti, and Zn were 0.02, 0.05, 0.02, 0.04, 0.03, and 0.05 μg/L, respectively. Laboratory reagent blanks (LRBs) were prepared and measured using the same procedures as for the samples except absence of the samples. At least one LRB was prepared and measured for each batch of up to 20 samples. One or more duplicated samples were analyzed for each type of sample and relative percent difference (RPD) was calculated to make sure good precision. RPDs ranged from 0 to 6%. Water reference standards purchased from High Purity co. were analyzed for each batch of samples. Laboratory sample spikes were also performed for each type of sample for ICP-MS analysis to make sure acceptable accuracy of analysis. The spike recoveries were ranged from 93 to 123%. During analysis, calibration checks with standard solutions were also performed frequently (every 10 – 12 samples) to monitor the instrument performance.

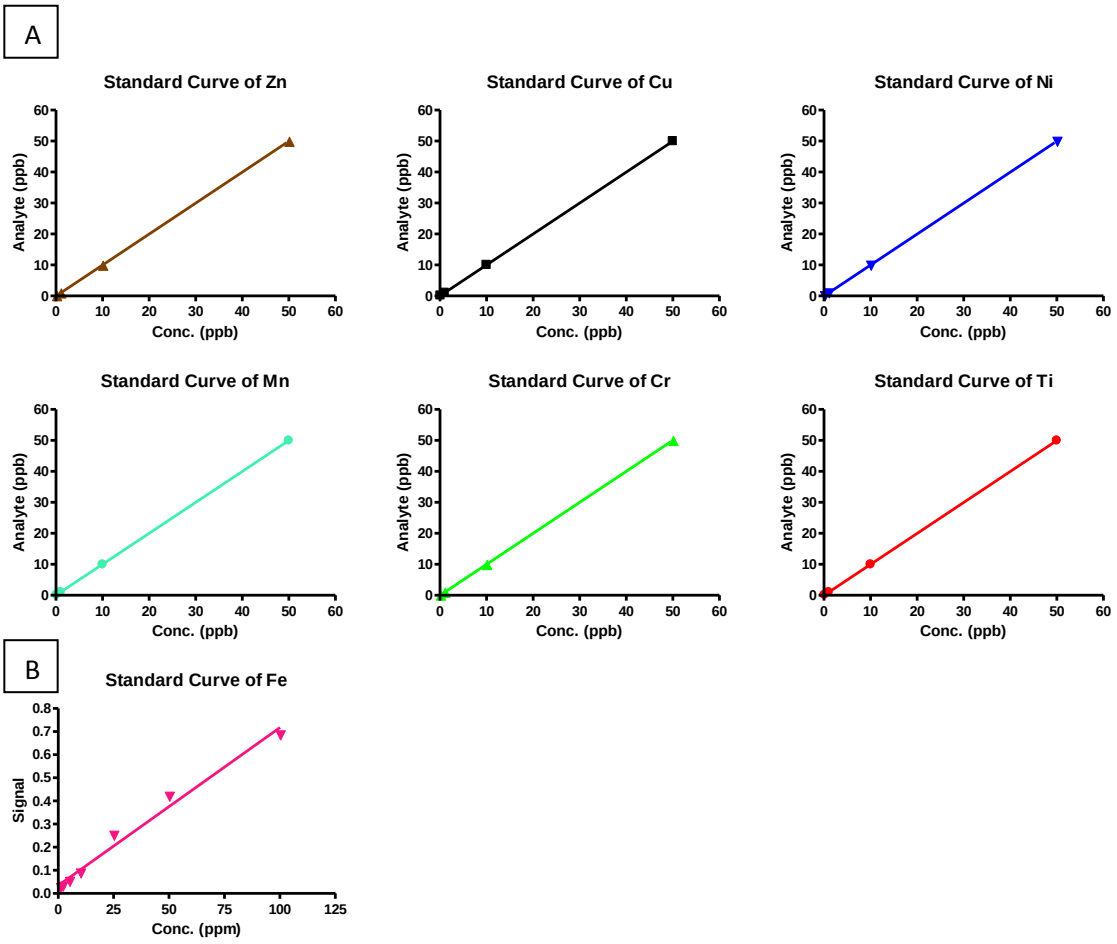

Figure 2.1: Reference standard curve. A.) the reference of element for ICP-MS which includes Zn, Cu, Ni, Mn, Cr, and Ti uses series concentration as 0.1, 1, 10, and 50 ppb for each element. The linear relationship between observation and reference of each element is analyzed and R^2 of each element is 1. B.) the reference of iron for GFFAS uses series concentration as 1, 2, 5, 10, 25, 50 and 100 ppb and the linear relationship between observation and reference of iron is analyzed. (R^2 =0.98).

2.10 STATISTICAL ANALYSIS

For cytotoxicity studies, three independent experiments were conducted, using triplicates for each treatment group. Data are expressed as mean ± standard error. For correlation between cytotoxicity and variables, such as APS, SSA, PZC, the number of available binding sites and dissolution, we employed spearman's correlation coefficient to analyze the relationship. All of the graphs were drawn by GraphPrism. Spearman's rank correlation coefficient is a nonparametric technique for evaluating the degree of correlation between two different variables. The nonparametric statistic is powerful when the assumptions of other statistical method are not met. The spearman's rank correlation coefficient does not depend on the size of sample, distribution of the population, and standard deviation of observations. Hence, it can be used with small sample size. Each variable is ranked from lowest to highest, such as 1, 2, 3, *etc*, and the difference between each ranked variable is calculated and squared. The spearman's rank correlation coefficient is calculated based on the following equation:

$$\rho = 1 - \frac{6\sum_{i=1}^{n} d_i}{n^3 - n}$$

$R_{xi} =$ rank of $x_i$value (x_i ranges from 1 to n, the smallest value is rank 1)

$R_{yi} =$ rank of y_i value (y_i ranges from 1 to n, the smallest value is rank 1)

$di = R_{xi} - R_{yi}\,, i = 1, 2, 3, \ldots \ldots, n$

n is the number of observation (sample size)

3. RESULTS

3.1 TRANSITION METAL OXIDES CHARACTERIZATION

Transition metal oxide nanoparticles, TiO_2, Cr_2O_3, Mn_2O_3, NiO, CuO and ZnO, were purchased from Nano structured and Amorphous Materials (99.9% purity; Los Alamos, New Mexico, USA). The manufacturing company provided the size range and SSA of the nanoparticles which is summarized in Table 3.1. It was essential to characterize the nanoparticles, investigate their morphology, and determine the particle size. TEM images of transition metal oxides as TiO_2, Cr_2O_3, Mn_2O_3, Fe_2O_3, NiO, CuO, and ZnO were shown in Figure 3.1A to Figure 3.7A, differential size distribution histogram were shown in Figure 3.1B to 3.7B and the APS was summarized in Table 3.1. The TiO_2 nanoparticles were spindle-shaped particles with an APS of 46 ± 20 nm which matched the information provided by the company (Figure 3.1). The Cr_2O_3 nanoparticles were spherically shaped with an APS of 63 ± 34 nm which agreed with the supplier (Figure 3.2). The Mn_2O_3 nanoparticles were spherical shape with an APS of 82 ± 31nm (Figure 3.3) which did not match the commercial size as 30-60 nm. Interestingly, most of the Mn_2O_3 nanoparticles were 75 to 100 nm with some particles located around 150 nm, yet APS was still within the 100 nm. The Fe_2O_3 nanoparticles were spherical in shape with an APS of 48 ± 13 nm (Figure 3.4). The NiO nanoparticles were spherical in shape and had an APS of 16 ± 5 nm (Figure 3.5). The CuO nanoparticles were spherical in shape and exhibited an APS of 47 ± 24 nm (Figure 3.6). The ZnO nanoparticles were spherical in shape with an APS of 27 ± 13 nm (Figure 3.7).

Overall, the morphology of the transition metal oxide nanoparticles was spherical in shape except the TiO_2 which was spindle shaped, and agglomeration was observed in each nanoparticle. Both TEM image and size distribution indicated that the size of nanoparticles ranged from 10 to 100 nm except that of Mn_2O_3 which had several particles that were around 150 nm. These results indicated that the information

Table 3.1: Measured morphology, APS and SSA of metal oxide nanoparticles

	TiO_2	**Cr_2O_3**	**Mn_2O_3**	**Fe_2O_3**	**NiO**	**CuO**	**ZnO**
SSA (m^2/g)	178.95	11.41	8.71	31.44	70.86	9.02	44.61
APS (nm)	46 ± 20	63 ± 34	82 ± 31	48 ± 13	16 ± 5	47 ± 24	27 ± 13
Morphology	rod-like shapes	roughly spherical	roughly spherical	roughly spherical	roughly spherical	roughly spherical	spherical and rod-like shapes
Data sheet provided by company							
SSA (m^2/g)	160	N.A.	N.A.	40	50-80	N.A.	50
APS (nm)	50	60	30-60	20-30	10-20	30-50	20

[N.A. denote not available]

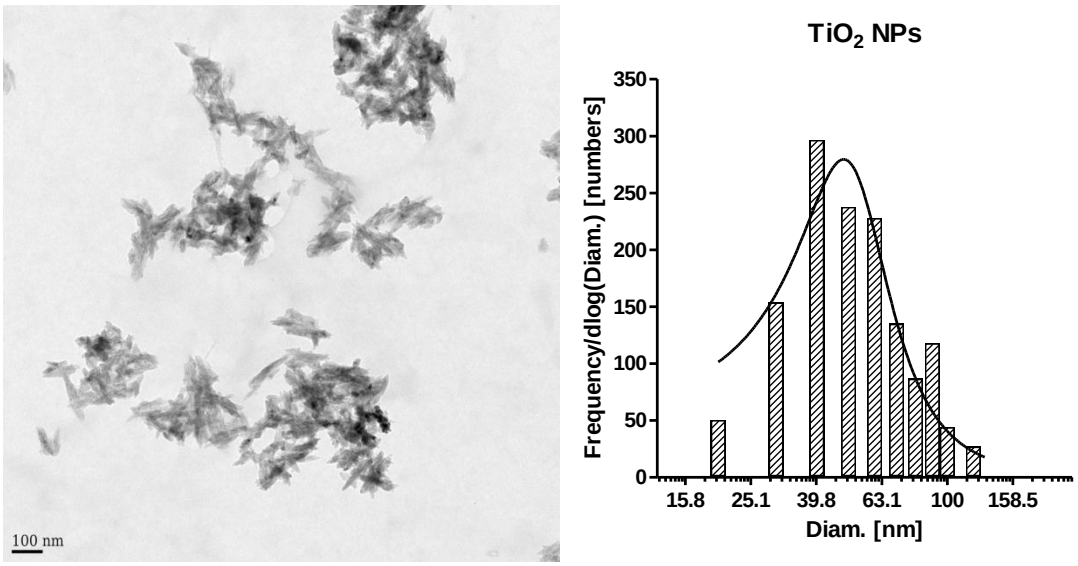

A **B**

Figure 3.1: (A) TEM image of TiO2 nanoparticles with (B) size histogram. Scale bar is 100 nm.

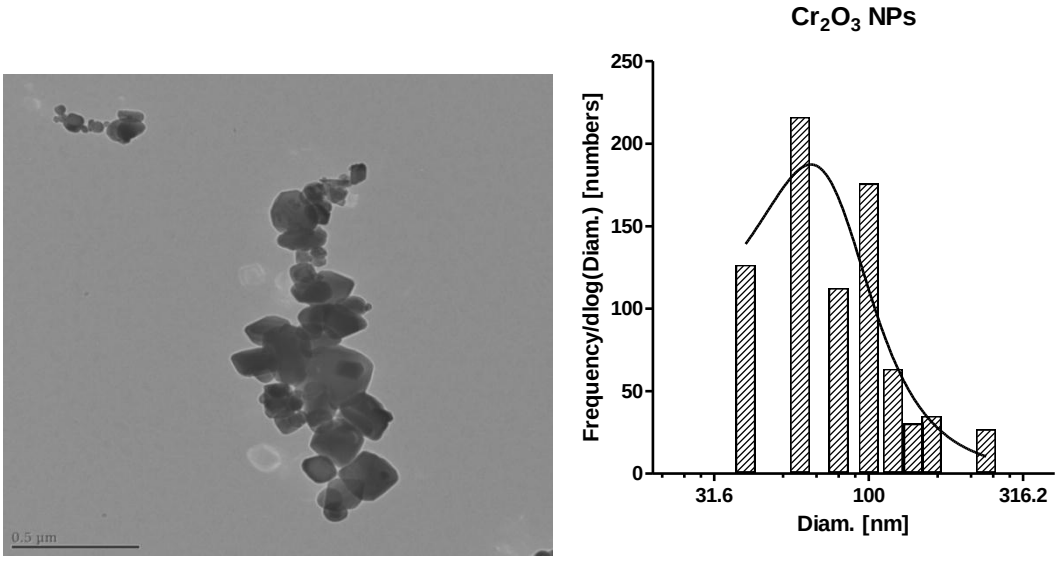

A **B**

Figure 3.2: (A) TEM image of Cr2O3 nanoparticles with (B) size histogram. Scale bar is 500 nm.

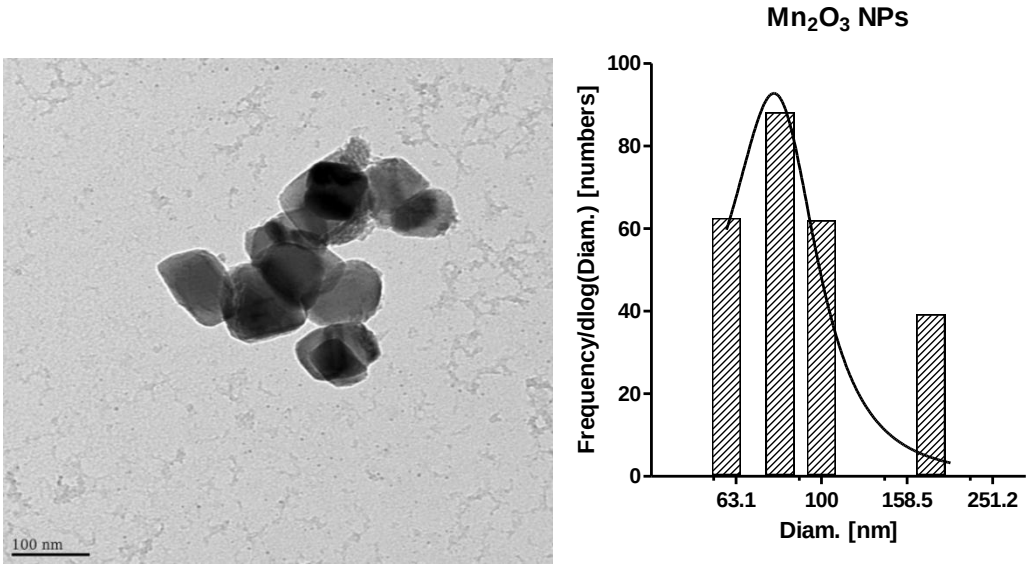

A **B**

Figure 3.3: (A) TEM image of Mn2O3 nanoparticles with (B) size histogram. Scale bar is 100 nm.

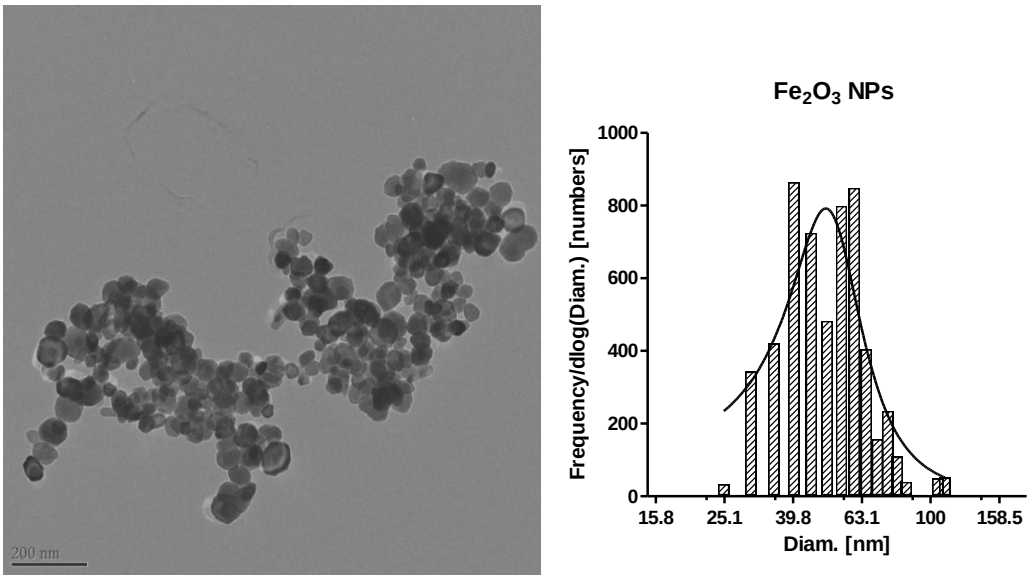

A **B**

Figure 3.4: (A) TEM image of Fe2O3 nanoparticles with (B) size histogram. Scale bar is 200 nm.

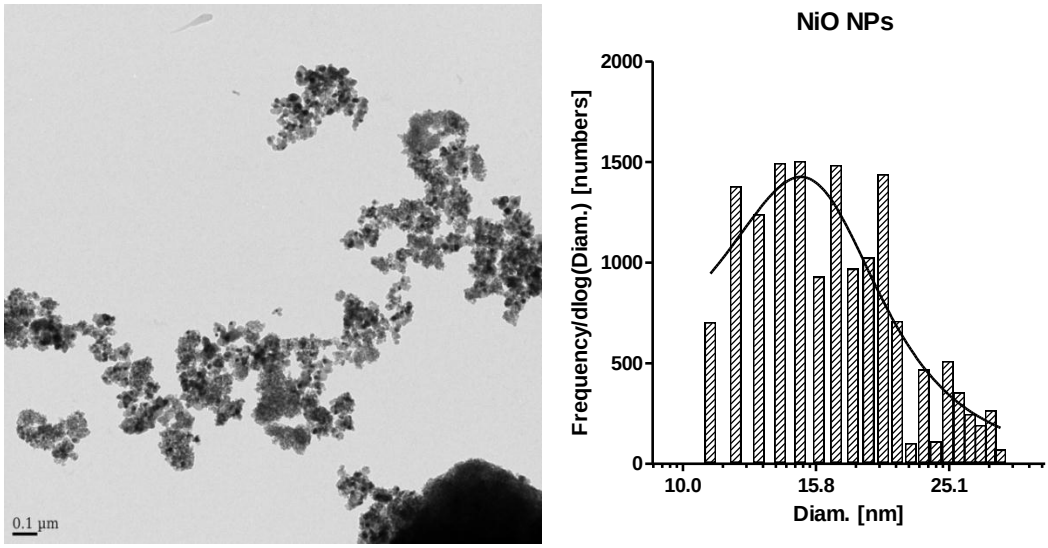

A B

Figure 3.5: (A) TEM image of NiO nanoparticles with (B) size histogram. Scale bar is 100 nm.

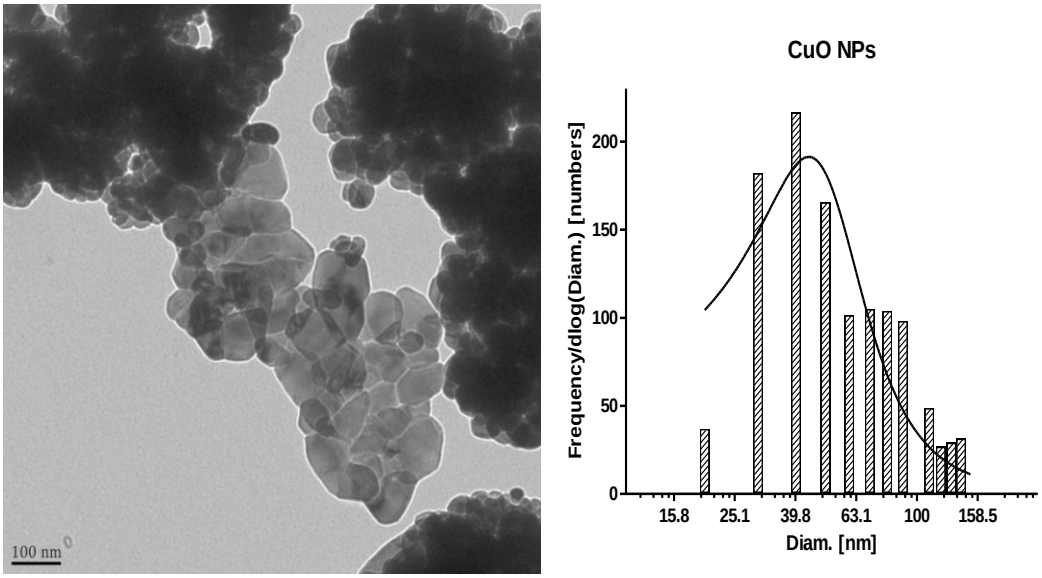

A B

Figure 3.6: (A) TEM image of CuO nanoparticles with (B) size histogram. Scale bar is 100 nm.

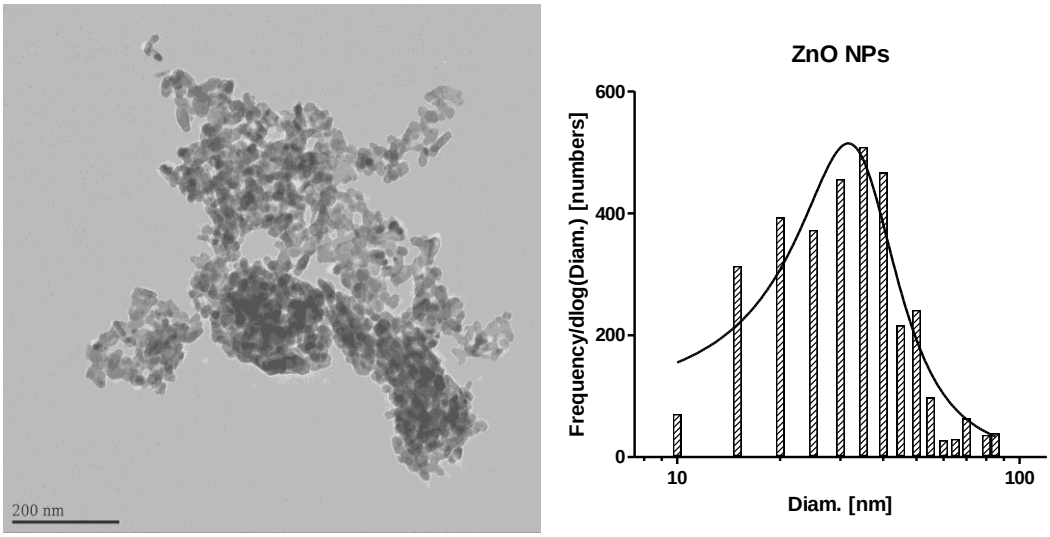

Figure 3.7: (A) TEM image of ZnO nanoparticles with (B) size histogram. Scale bar is 200 nm.

provided by company matched the data from our study. In Figure 3.1B to 3.7B, the size distribution of each transition metal oxide which matched the fitted line suggested that the size of each nanoparticle followed a normal distribution. Furthermore, we use spearman's rank correlation coefficient to demonstrate the correlation between cytotoxicity and APS. There is a weak correlation between cytotoxicity and APS (spearman's rank correlation coefficient, $\rho = -0.32$) (Figure 3.8).

The specific surface area (SSA) measurements of all seven transition metal oxide nanoparticles were obtained by BET method [68] and the data are included in Table 2. The specific surface area (m^2/g) was the surface area divided by unit gram of the nanoparticles. We found that there is a weak correlation between cytotoxicity and SSA (spearman's rank correlation coefficient, $\rho = -0.32$) (Figure 3.9). In conclusion, the APS and SSA displayed little effect on the increasing cytotoxicity of transition metal oxides.

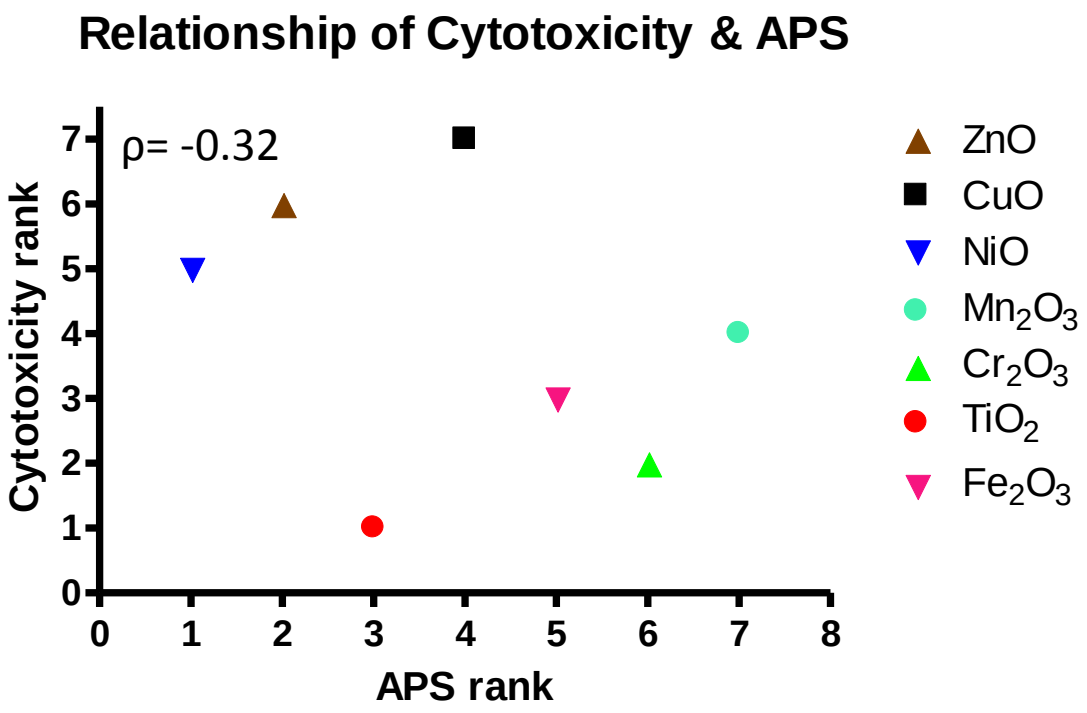

Figure 3.8: Relationship of cytotoxicity & APS. There is a weak correlation between cytotoxicity of transition metal oxides and APS (spearman's rank correlation coefficient, ρ = -0.32).

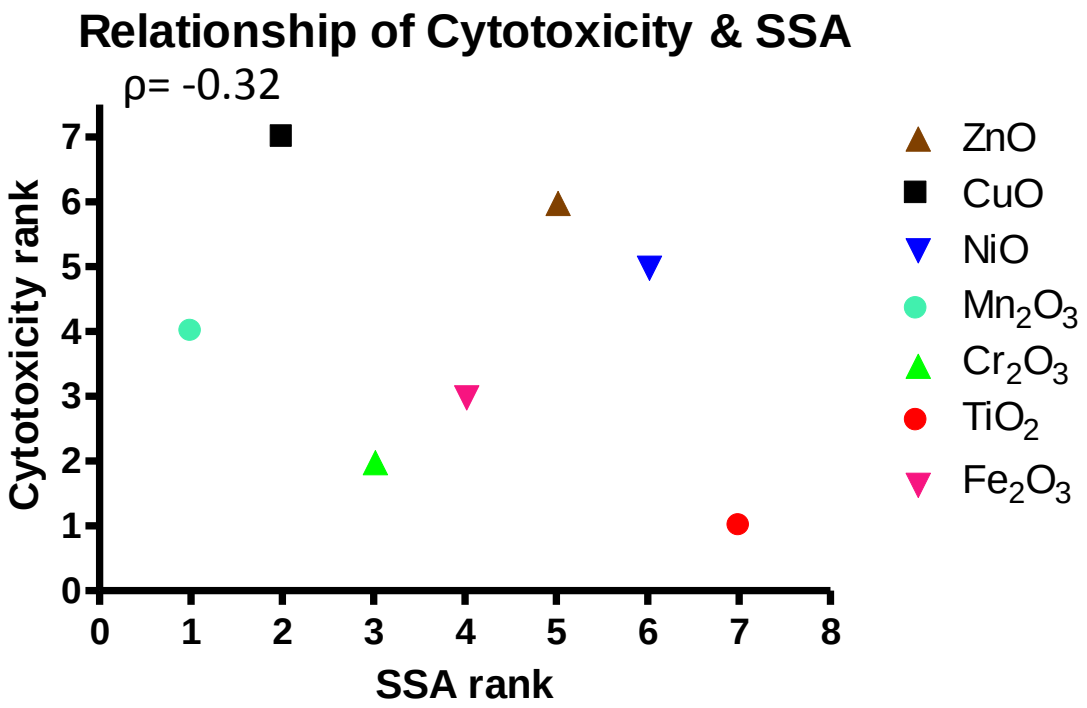

Figure 3.9: Relationship of cytotoxicity & SSA. There is a strong correlation between cytotoxicity of transition metal oxides and SSA (spearman's rank correlation coefficient, ρ = -0.32).

3.2 CYTOTOXICITY INCREASED AS ATOMIC NUMBER OF TRANSITION METAL OXIDE INCREASED

Dosimetry measurements were made on BEAS-2B cell lines based on four different setting of X-axis units: 1.) particle mass/medium volume, 2.) particle mass/seeding area, 3.) particle specific surface area/seeding area, 4.) particle specific surface area/medium volume were and are summarized in Figure 3.10. The same type of measurements on A549 cell lines are shown in Figure 3.11. Within these four plots with different X-axis units, the trend of cytotoxicity was similar with the exception of Mn_2O_3 (Figure 3.10 and Figure 3.11). The cells (BEAS-2B and A549, respectively) were treated with series concentration of seven transition metal oxides for 24 hr. Greater percent cell viability, relative to the control group, denotes less cytotoxicity of the nanoparticles. In the case of BEAS-2B cell lines, the degree of cytotoxicity based on mass/medium volume had the following trend: $TiO_2 < Cr_2O_3 < Fe_2O_3 < Mn_2O_3 <$ NiO < ZnO < CuO. The trend matches the periodicity of the transition metal within the metal oxides with the exception of Mn_2O_3. In accordance with the cell viability of each metal oxide (Figure 3.10 and Figure 3.11), the transition metal oxides were defined as three degrees of cytotoxicity: none-to-minor, moderate, and steep. TiO_2, Cr_2O_3, and Fe_2O_3 were concluded to possess none-to-minor cytotoxicity; Mn_2O_3 and NiO were concluded to have moderate cytotoxicity; and ZnO and CuO were concluded to exhibit steep cytotoxicity. The degree of cytotoxicity increased as none-to-minor > moderate > steep while the atomic number of nanoparticles went up with the exception of Mn_2O_3. There is a strong correlation between cytotoxicity and atomic number (spearman's rank correlation coefficient, $\rho = 0.93$) (Figure 3.12). Compared with the cytotoxicity of transition metal oxide treated in BEAS-2B and A549, the result showed that the cytotoxicity is not cell type specific. In conclusion, the cytotoxicity increased as the atomic number of nanoparticle increased.

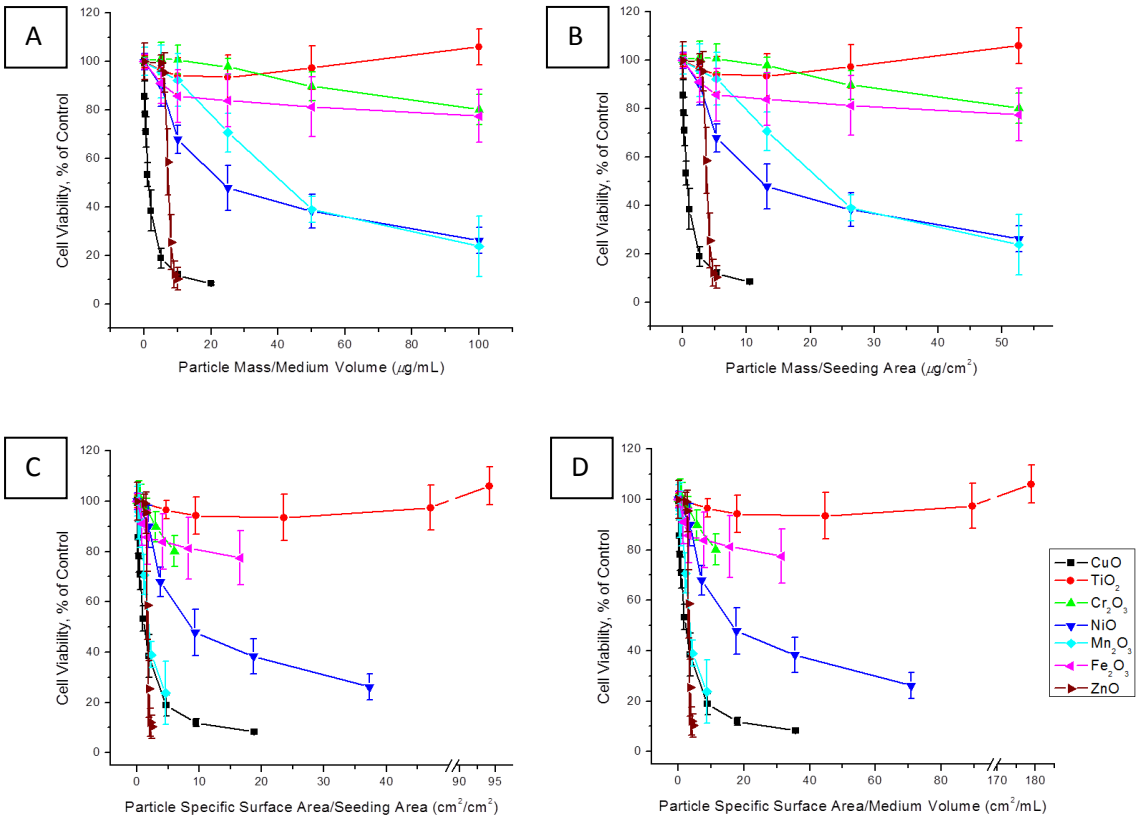

Figure 3.10: Cytotoxicity of seven transition metal oxides in BEAS-2B cells exposed for 24 hr. A.) The X axis is plotted based on mass/medium volume. B.) The X axis is plotted based on mass/seeding area. C.) The X axis is plotted based on surface area/seeding area. D.) The X axis is plotted based on area/medium volume.

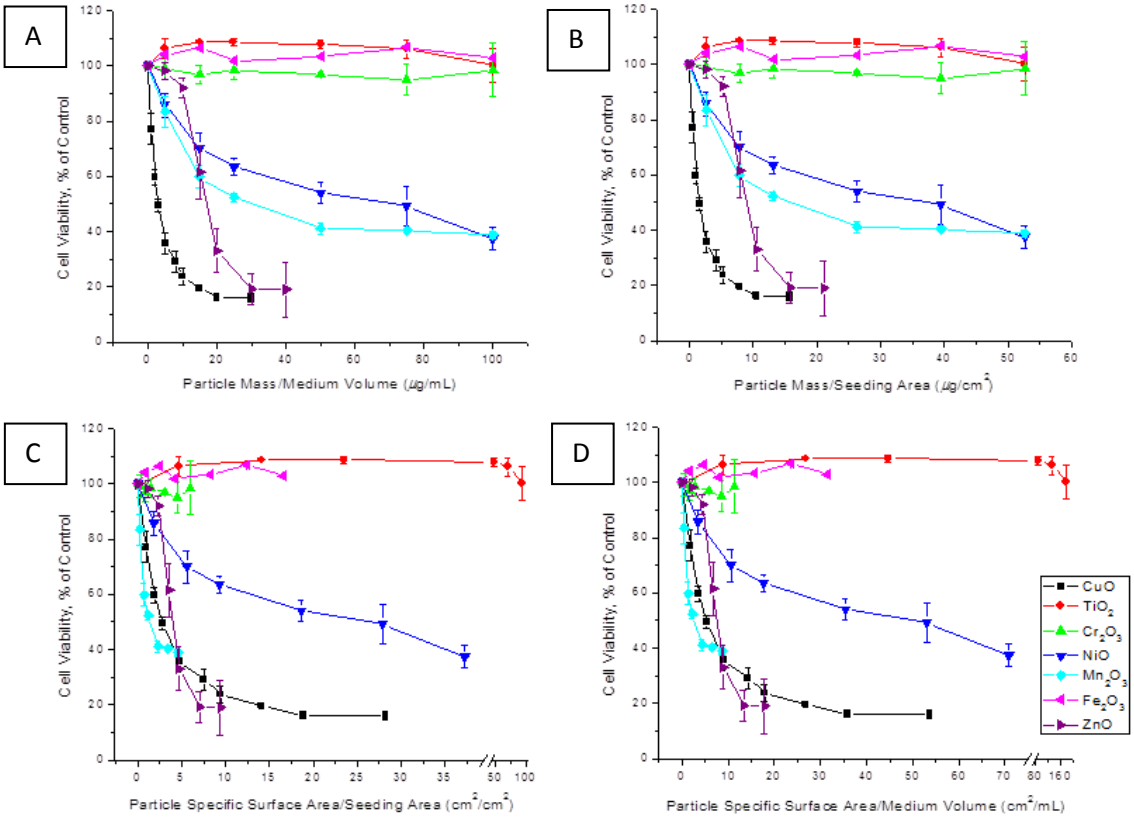

Figure 3.11: Cytotoxicity of seven transition metal oxides in A549 cells exposed for 24 h. A.) The X axis is plotted based on mass/medium volume. B.) The X axis is plotted based on mass/seeding area. C.) The X axis is plotted based on surface area/seeding area. D.) The X axis is plotted based on area/medium volume.

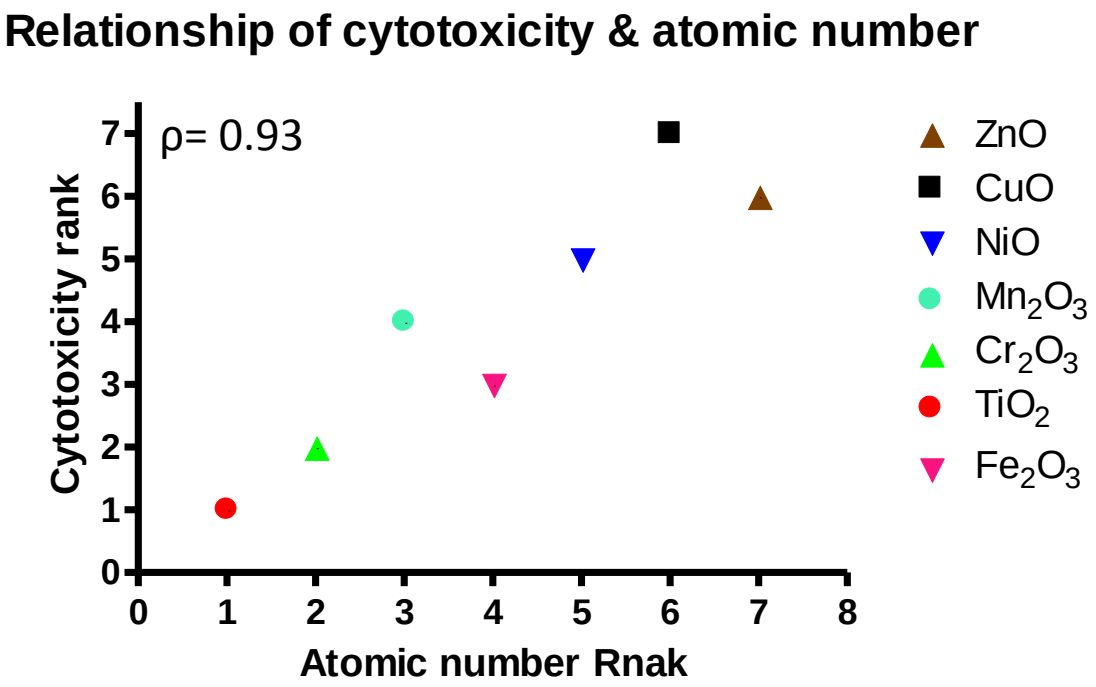

Figure 3.12: Relationship of cytotoxicity & atomic number. There is a strong correlation between cytotoxicity of transition metal oxides and the atomic number (spearman's rank correlation coefficient, ρ = 0.93).

3.3 THE CORRELATION BETWEEN PZC AND CYTOTOXICITY

PZC was shown in Figure 3.13 and summarized in Table 3.2. With the exception of Mn_2O_3, a higher PZC corresponded with greater cytotoxicity. The horizontal dashed lines denote physiological pH at 7.4 and 4.5 (Figure 3.13). The pH value in cytosol environment is referenced to be 7.4, whereas the pH value is 4.5 in lysosome. Notably, we observed a potential threshold at pH = 8.0. Mn_2O_3, NiO, CuO, and ZnO had a PZC above 8.0 (PZC value: 8.8, 8.2, 8.5 and 8.5, respectively) and were defined as moderate and steep cytotoxicity. And the none-to-minor cytotoxic nanoparticles, i.e TiO_2, Cr_2O_3, and Fe_2O_3 had PZC below 8.0 as 6.8, 7.8 and 8.0, respectively. There is a strong correlation between cytotoxicity and PZC (spearman's rank correlation coefficient, ρ = 0.78) (Figure 3.14). In conclusion, the cytotoxicity of nanoparticles increased as the PZC value rose.

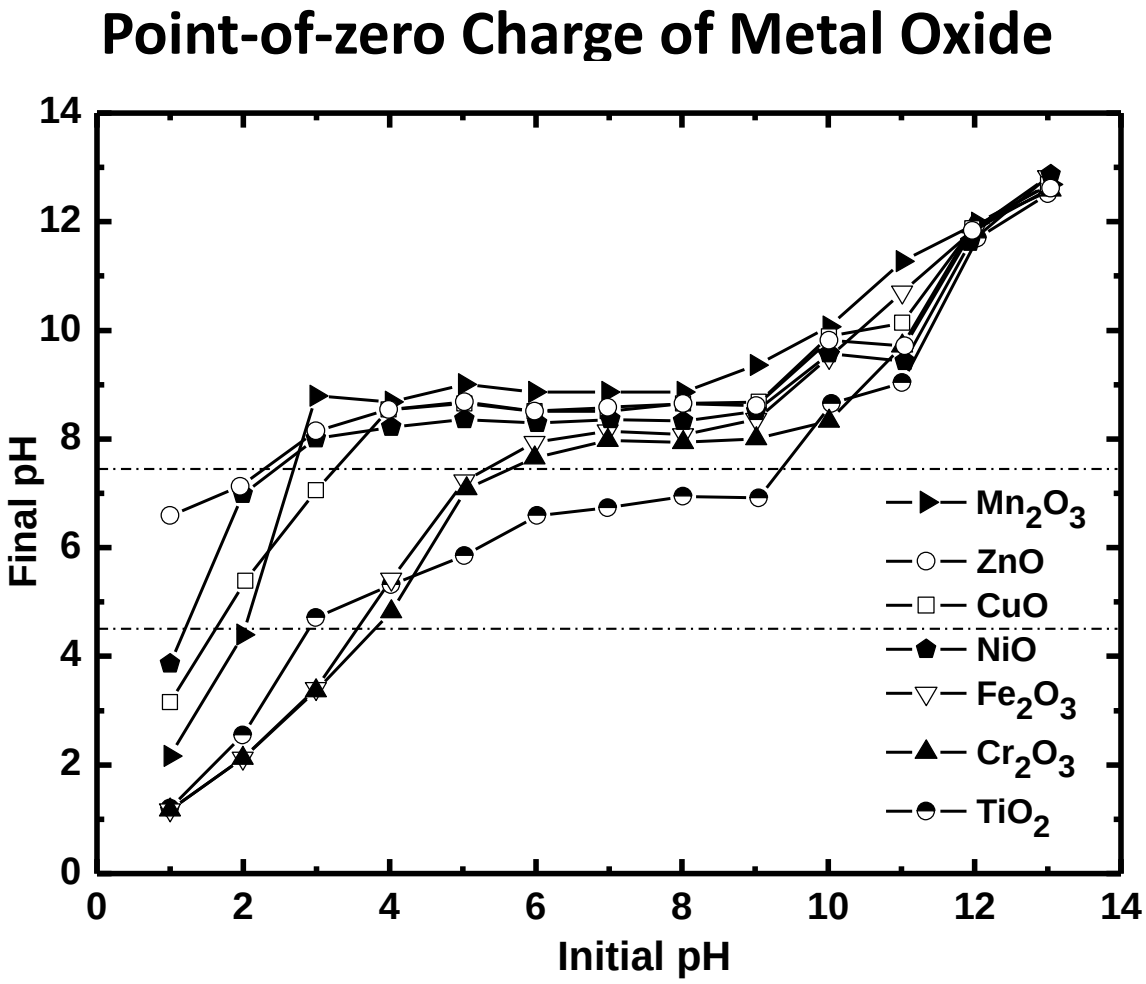

Figure 3.13: PZC initial pH against final pH plots of transition metal oxides including Mn_2O_3, ZnO, CuO, NiO, Fe_2O_3, Cr_2O_3 and TiO_2. Vertical dashed line denotes physiological pH = 4.5 and 7.4, respectively.

Table 3.2: Physicochemical properties showing correlation with cytotoxicity

Atomic no. of metal	Metal oxide NP	Cell viability	PZC	Physisorbed-to-metal oxide oxygen	% dissolved in solution (pH 7.4)	% dissolved in solution (pH 4.5)
22	TiO_2	100.0%	6.8	0.56	0.00012%	0.00010%
24	Cr_2O_3	80.1%	7.8	3.09*	0.00507%	0.00200%
25	Mn_2O_3	29.6%*	8.8*	0.71	0%	0%
26	Fe_2O_3	79.9%	8.0	1.06	0.00822%	0.46930%
28	NiO	29.9%	8.2	2.33	0.23699%	2.32698%
29	CuO	9.8%	8.5	6.64	0.47672%	11.41012%
30	ZnO	10.0%	8.5	6.76	0.46229%	26.08621%

[Asterisks * denote deviation to periodic trend]

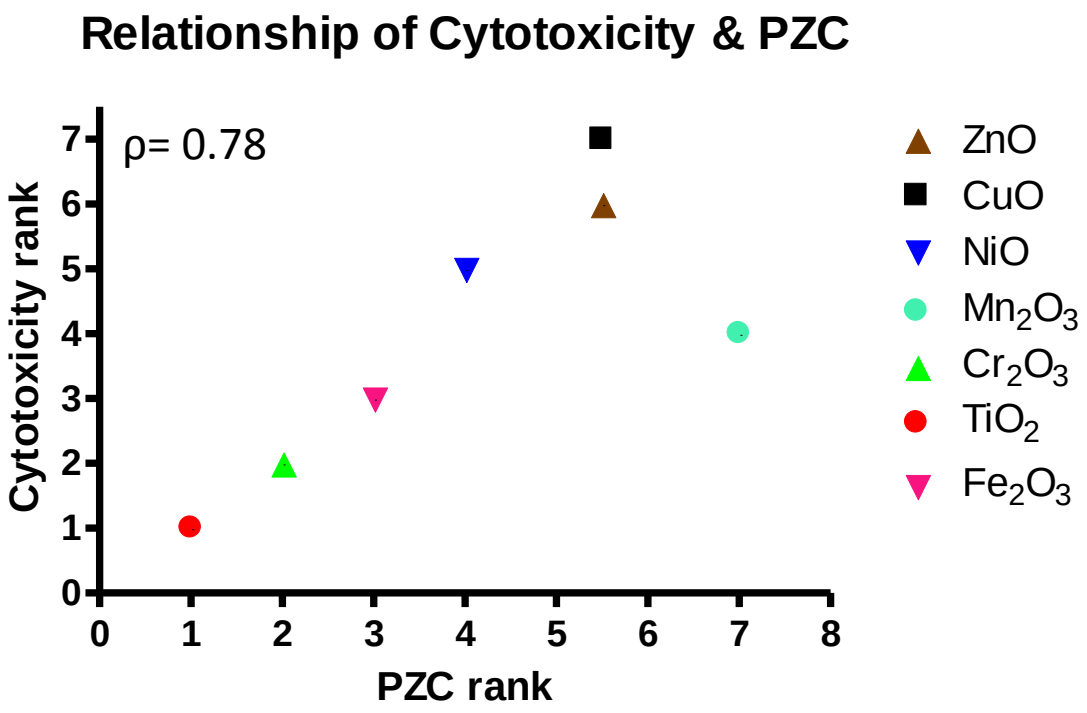

Figure 3.14: Relationship of cytotoxicity & PZC. There is a strong correlation between cytotoxicity of transition metal oxides and PZC (spearman's rank correlation coefficient, ρ = 0.78).

3.4 THE CORRELATION BETWEEN THE NUMBER OF AVAILABLE BINDING SITES AND CYTOTOXICTY

In addition to the observed trend in PZC, a periodicity in the number of available binding sites, as measured by XPS, was shown to be correlated with cytotoxicity trends (Figure 3.15). The relative adsorbed oxygen-to-metal oxide ratio, obtained from integrated XPS peak areas, was used as a means of quantifying the number of available binding sites to which intracellular material can interact via attachment. The greater the physisorbed- oxygen-to-metal oxide ratio is, the more adsorption sites are available for intracellular binding. The peak assignment was done by matching the calculated binding energies with experimentally determined binding energy values. The NIST X-ray photoelectron spectroscopy database (http://srdata.nist.gov/xps/, version 3.5) was used. Figure 3.15A showed a stack plot of XPS spectra of the O 1s orbitals of the Fe_2O_3, Mn_2O_3 and TiO_2 nanoparticles following a 16-hr CC reaction in a pH = 7.4 environment. The chemical oxidation state denoting metal oxide (blue traces in Figure 3.15) was clearly defined. XPS binding energies (BE) at 530.0 eV, 529.6 eV and 529.5 eV match literature values for the oxide oxidation state for TiO_2 [69], Mn_2O_3 [70] and Fe_2O_3 [71], respectively. BEs observed at 531.9 eV on TiO_2, 530.9 eV and 531.5 eV on Mn_2O_3, and 530.6 eV on Fe_2O_3 are consistent with adsorbed hydroxyl species (OH^-) on these surfaces [72, 73]. Figure 3.15B similarly shows a stack plot of XPS spectra of the O 1s orbitals of NiO, Cr_2O_3, CuO and ZnO following the 16-hr CC reaction. BEs of the metal oxide chemical state observed at O 1s = 528.9, 529.6, 529.6 and 529.8 eV, matched their literature values for NiO [74], Cr_2O_3 [75], CuO [76] and ZnO [71], respectively. BE peaks centered at 532.9 eV, 531.1, and 532.6 eV on CuO were also consistent with the presence of adsorbed oxygen from hydroxyl species (OH^-) [77]. BE peaks centered at 530.7 eV and 532.5 eV on Cr_2O_3, and 531.6 eV on ZnO were also consistent with the presence of adsorbed carbonyl group (C=O) [78, 79]. BE peaks centered at 531.0 eV on NiO was assigned to adsorbed oxygen from carbonate[69]. There is a strong correlation between cytotoxicity and the number of available binding sites (spearman's rank correlation coefficient, $\rho = 0.71$) (Figure 3.16).

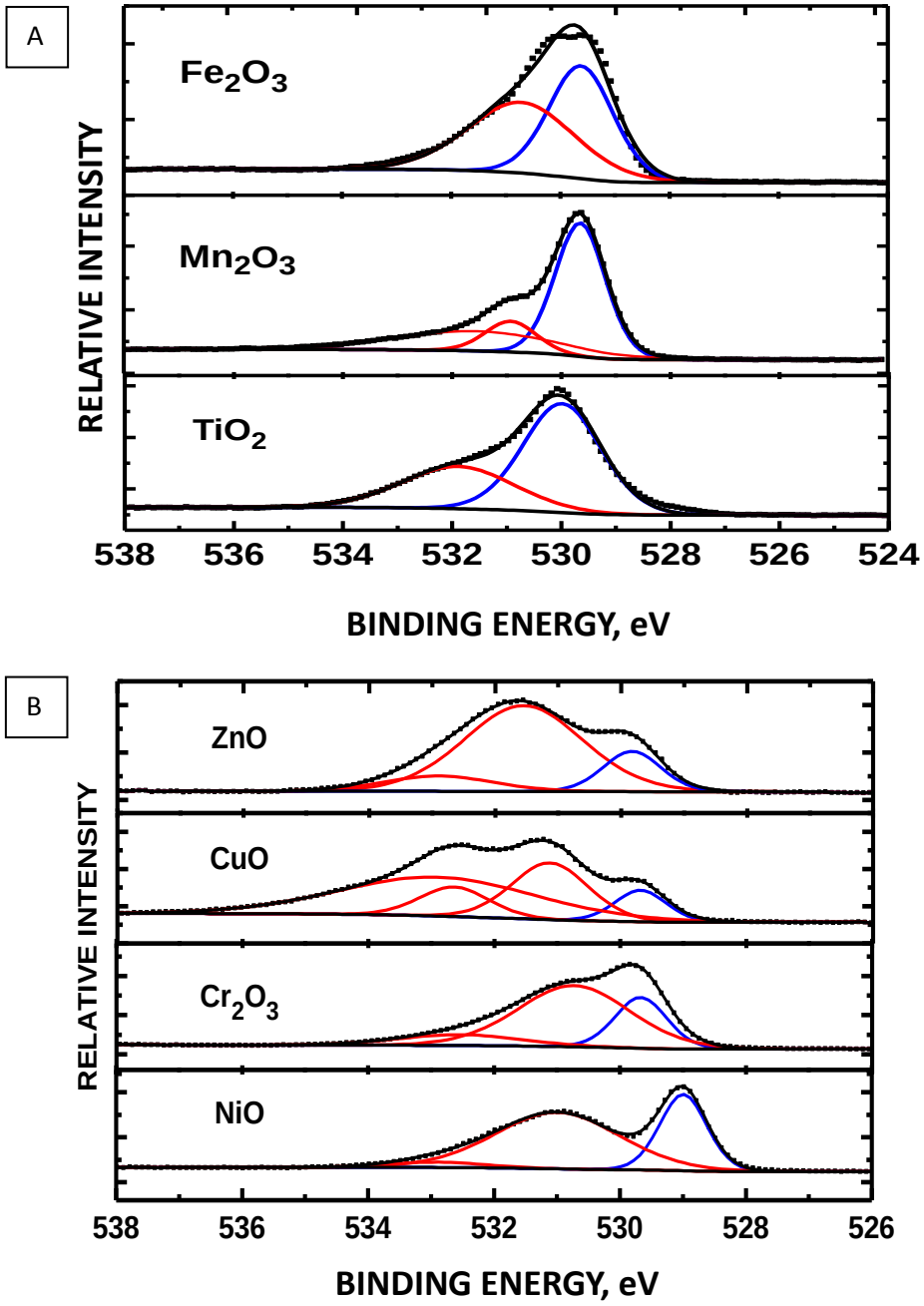

Figure 3.15: XPS of O 1s orbitals of transition metal oxide. A.) XPS of O 1s orbitals of Fe_2O_3, Mn_2O_3 and TiO_2 metal oxide nanoparticles. Blue envelopes denote metal oxide chemical oxidation state. B.)XPS of O 1s orbitals of ZnO, CuO, Cr_2O_3 and NiO metal oxide nanoparticles. Blue envelopes denote metal oxide chemical oxidation state. Red envelopes denoted adsorbed oxygen. Vertical dashed line denotes BE position for adsorbed H_2O.

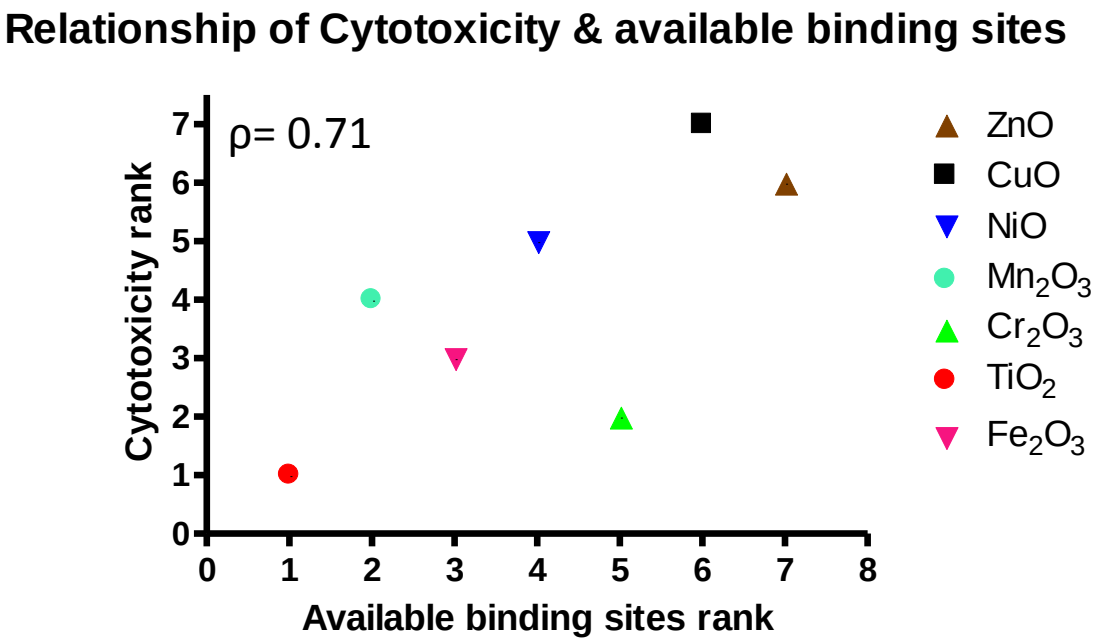

Figure 3.16: Relationship of cytotoxicity & the number of available binding sites. There is a strong correlation between cytotoxicity of transition metal oxides and the number of available binding sites (spearman's rank correlation coefficient, ρ = 0.71).

3.5 THE CORRELATION BETWEEN METAL DISSOLUTION OF TRANSITION METAL OXIDES AND CYTOTOXICITY

Following the evaluation correlation between nanoparticle surface binding sites and cytotoxicity, the metal dissolution of metal oxides was further examined. The metal dissolution of seven transition metal oxides in pH 4.5 and 7.4 was summarized in Table 3.3. The samples were collected in two different pH environments, 4.5 and 7.4, at 6, 12, 18, 24 hr. Inside the cell, a stable and consistent physiological condition, such as pH value, is maintained to provide a favorable metabolic environment. In our model, nanoparticles could interact with H_2O to alter the pH value. To resolve this issue of pH shift by nanoparticles, autotitration was employed to maintain a stable and consistent pH value in cytosol and lysosome of 4.5 and 7.4, respectively.

The ZnO nanoparticle had an average metal dissolution of 25% from four time points (6, 12, 18, and 24 hour) at pH 4.5 and 0.47% dissolution at pH 7.4. This result demonstrated that the ZnO nanoparticles tend to release more Zinc ion under acidic conditions. The dissolution of ZnO nanoparticle did not show an increasing trend as time passed by (Figure 3.17). The CuO nanoparticle had an average dissolution 11% over four time points at pH 4.5 and 0.47% dissolution at pH 7.4. The result showed that the CuO nanoparticles tend to release more copper ions under acidic conditions. The dissolution of CuO nanoparticle did not show an increasing trend as time passed by (Figure 3.18). Interestingly, the dissolution of ZnO and CuO at pH 7.4 had identical value of 0.47%. The dissolution of NiO had an average value of 2% over four time points at pH 4.5 and 0.2% at pH 7.4. This showed the NiO nanoparticle tended to release nickel ions under acidic conditions. Also, the dissolution of NiO nanoparticles did not show an increasing trend with time (Figure 3.19). The dissolution of Mn_2O_3 had an average value 0.5% over four time points at pH 4.5 and was below 0.01% at pH 7.4. This showed that the Mn_2O_3 nanoparticle's ability to release manganese ions under acidic conditions slightly increased. Also, the dissolution of the Mn_2O_3 nanoparticles did not show an increasing trend with time (Figure 3.20). The dissolution of Fe_2O_3, Cr_2O_3 and TiO_2 nanoparticles was below 0.01% which is summarized in table 3.3.

In summary, the dissolution of all seven nanoparticles at pH 7.4 was less than 1% (Table 3.3) and this result indicates that nanoparticles exposed in cytosol environment would not release metal ions. There is a strong correlation between cytotoxicity and dissolution at pH 7.4 (spearman's rank correlation coefficient, $\rho = 0.89$) (Figure 3.21A). The metal dissolution of nanoparicltes at pH 4.5 showed various results ranging from 0 to 25 % with different nanoparticles. At the pH 4.5 condition, ZnO and CuO, which exhibited sever cytotoxicity, had the highest dissolution rate of nearly 25% and 11% respectively; NiO and Mn_2O_3, which exhibit mild cytotoxicity, displayed a 2% and 0.5% dissolution rate, respectively; Fe_2O_3, Cr_2O_3, and TiO_2, which exhibit minor cytotoxicity, had dissolution below 0.1%. On the other hand, the dissolution of all seven nanoparticles at pH 7.4 had values below 1%. There is a strong correlation between cytotoxicity and dissolution at pH 4.5 (spearman's rank correlation coefficient, $\rho = 0.86$) (Figure 3.21B).

Table 3.3: Metal dissolution of transition metal oxide

Metal oxide	pH value	Time (hour)	Dissolution (%)
ZnO	7.4	6	**0.36497%**
		12	**0.43795%**
		18	**0.99180%**
		24	**0.04946%**
	4.5	6	**25.94597% ± 4.98%**
		12	**31.54751% ± 0.50%**
		18	**31.99241% ± 12.72%**
		24	**14.99871% ± 6.06%**
CuO	7.4	6	**0.02138%**
		12	**0.15414%**
		18	**0.00852%**
		24	**1.72286%**
	4.5	6	**6.84158% ± 0.29%**
		12	**9.85740% ± 1.14%**
		18	**14.97398% ± 6.16%**
		24	**13.96753% ± 2.29%**
NiO	7.4	6	**0.09015%**
		12	**0.40732%**
		18	**0.19613%**
		24	**0.25434%**
	4.5	6	**3.99964%**
		12	**2.18469%**
		18	**1.29370%**
		24	**1.82991%**
Mn_2O_3	7.4	6	**0.00201%**
		12	**0.00067%**
		18	**0.00683%**
		24	**0.02323%**
	4.5	6	**0.40881%**
		12	**0.29667%**
		18	**0.55140%**
		24	**0.62015%**

Table 3.3: Metal dissolution of transition metal oxide (cont.)

Fe_2O_3	7.4	6	**0.00000%**
		12	**0.00000%**
		18	**0.00000%**
		24	**0.00000%**
	4.5	6	**0.00000%**
		12	**0.00000%**
		18	**0.00000%**
		24	**0.00000%**
Cr_2O_3	7.4	6	**0.00399%**
		12	**0.00494%**
		18	**0.00539%**
		24	**0.00597%**
	4.5	6	**0.00136%**
		12	**0.00188%**
		18	**0.00219%**
		24	**0.00257%**
TiO_2	7.4	6	**0.00010%**
		12	**0.00008%**
		18	**0.00012%**
		24	**0.00007%**
	4.5	6	**0.00009%**
		12	**0.00002%**
		18	**0.00007%**
		24	**0.00009%**

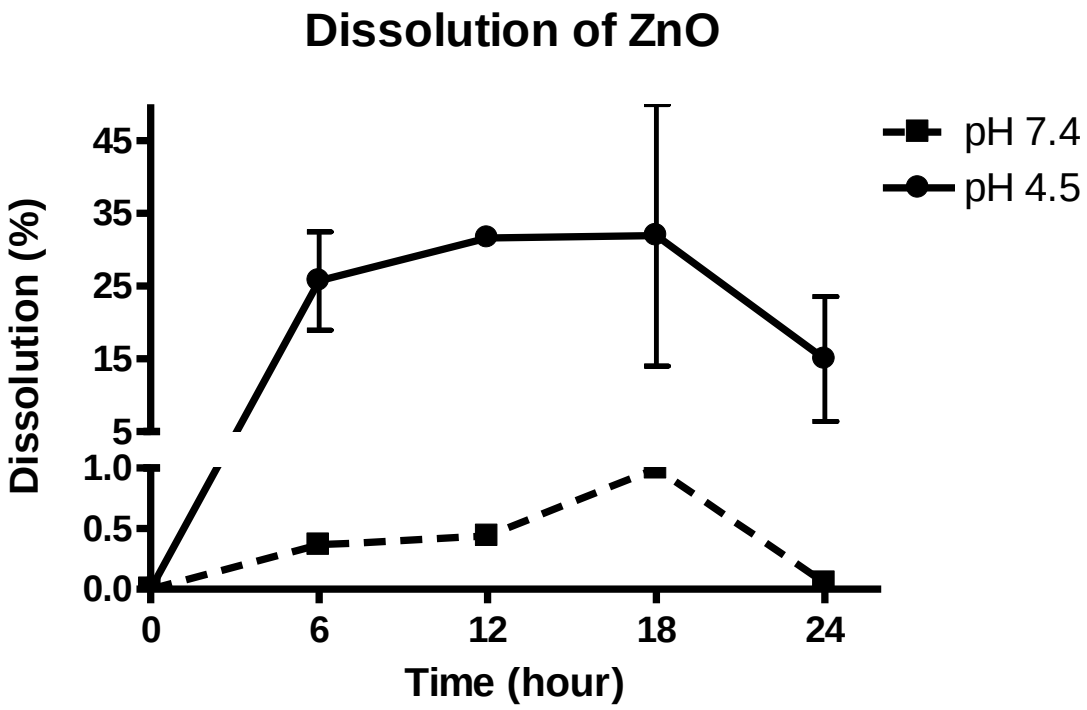

Figure 3.17: Dissolution of ZnO. ZnO was added into 0.01 M NaCl solution maintaining pH at 7.4 and 4.5, respectively. 250 mg of ZnO was dispersed into 50 mL 0.01 M NaCl solution. At each time point (6, 12, 18 and 24 hr), the 4 mL of sample was taken out and centrifuged for 5 min at at 4^{o}C, 12,000 rpm for 5 min. The supernatant of solution was further transferred into dialysis membrane and wait for 17 hr. After dialysis, the sample was analyzed by ICP-MS. Values are mean $\pm$ SD from two independent experiments.

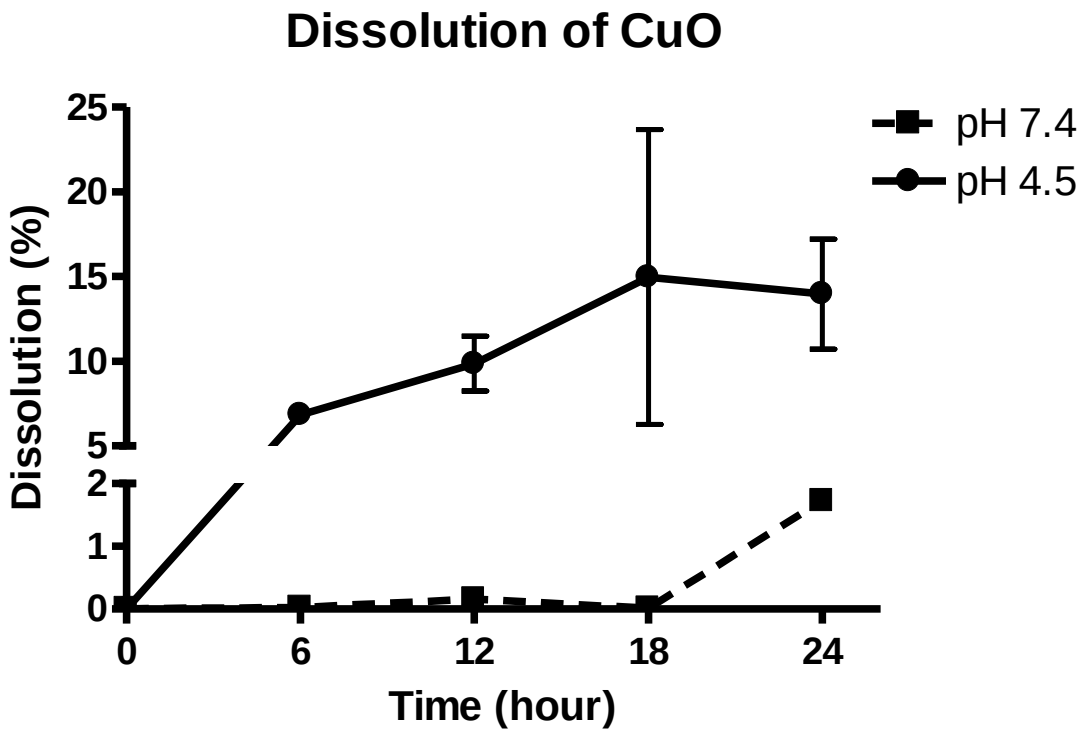

Figure 3.18: Dissolution of CuO. CuO was added into 0.01 M NaCl solution maintaining pH at 7.4 and 4.5, respectively. 250 mg of CuO was dispersed into 50 mL 0.01 M NaCl solution. At each time point (6, 12, 18 and 24 hr), the 4 mL of sample was taken out and centrifuged for 5 min at at 4^{o}C, 12,000 rpm for 5 min. The supernatant of solution was further transferred into dialysis membrane and wait for 17 hr. After dialysis, the sample was analyzed by ICP-MS. Values are mean $\pm$ SD from two independent experiments.

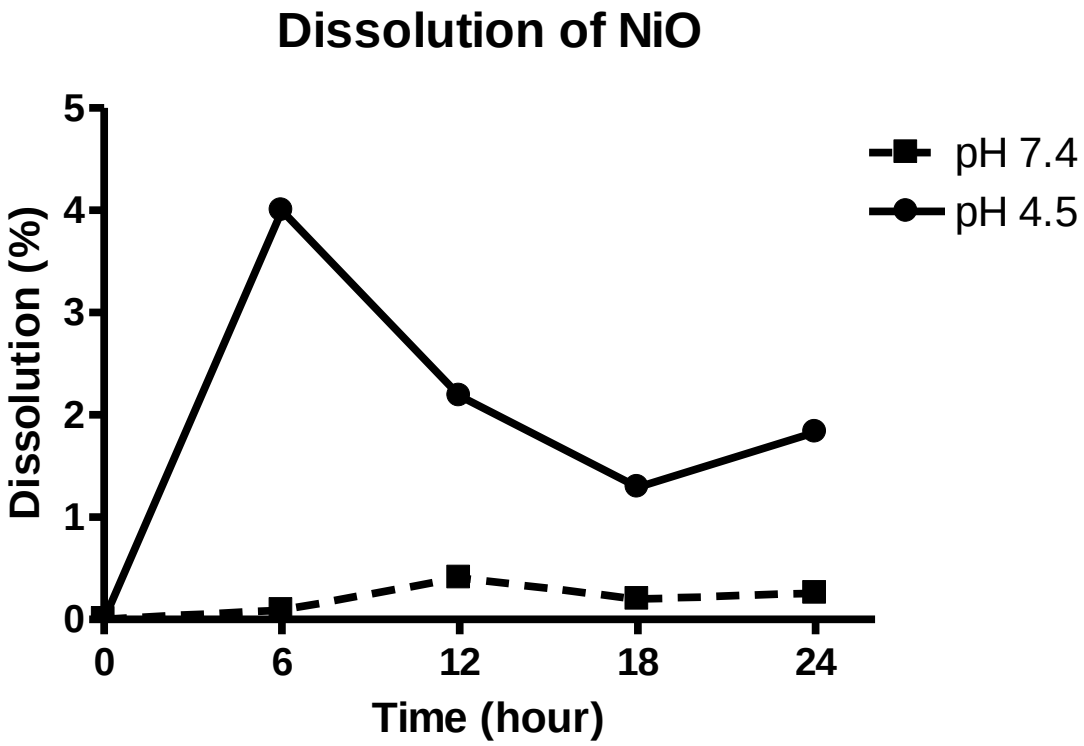

Figure 3.19: Dissolution of NiO. NiO was added into 0.01 M NaCl solution maintaining pH at 7.4 and 4.5, respectively. 250 mg of NiO was dispersed into 50 mL 0.01 M NaCl solution. At each time point (6, 12, 18 and 24 hr), the 4 mL of sample was taken out and centrifuged for 5 min at at 4^{o}C, 12,000 rpm for 5 min. The supernatant of solution was further transferred into dialysis membrane and wait for 17 hr. After dialysis, the sample was analyzed by ICP-MS.

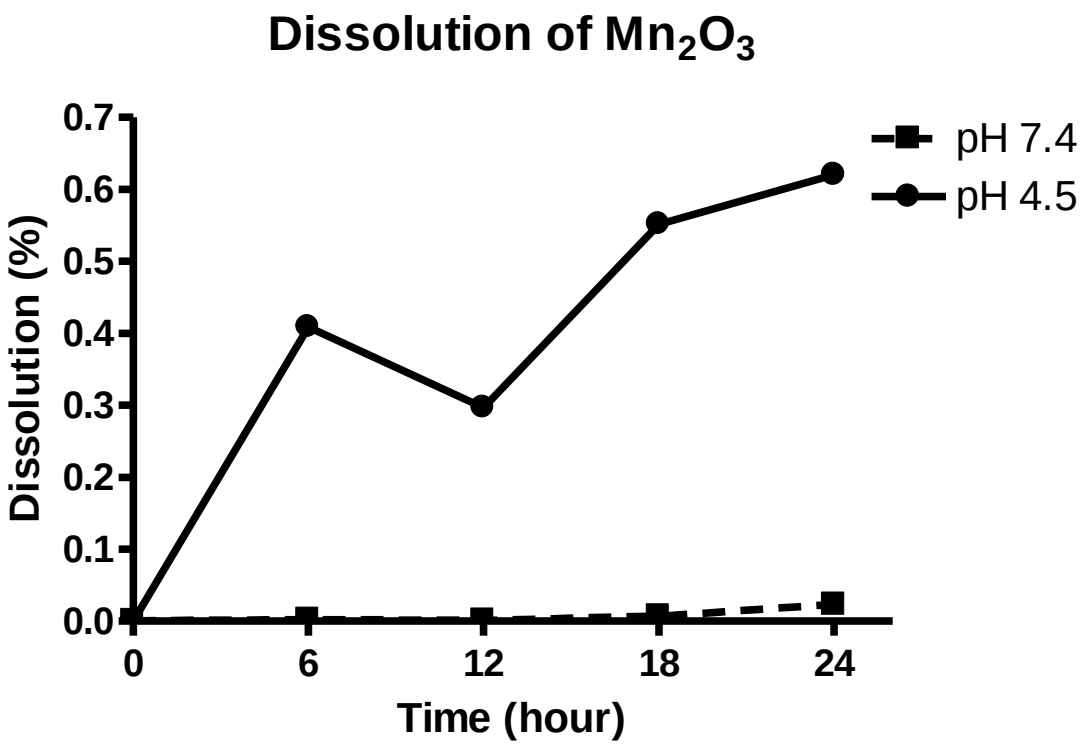

Figure 3.20: Dissolution of Mn_2O_3. Mn_2O_3 was added into 0.01 M NaCl solution maintaining pH at 7.4 and 4.5, respectively. 250 mg of Mn_2O_3 was dispersed into 50 mL 0.01 M NaCl solution. At each time point (6, 12, 18 and 24 hr), the 4 mL of sample was taken out and centrifuged for 5 min at at 4^{o}C, 12,000 rpm for 5 min. The supernatant of solution was further transferred into dialysis membrane and wait for 17 hr. After dialysis, the sample was analyzed by ICP-MS.

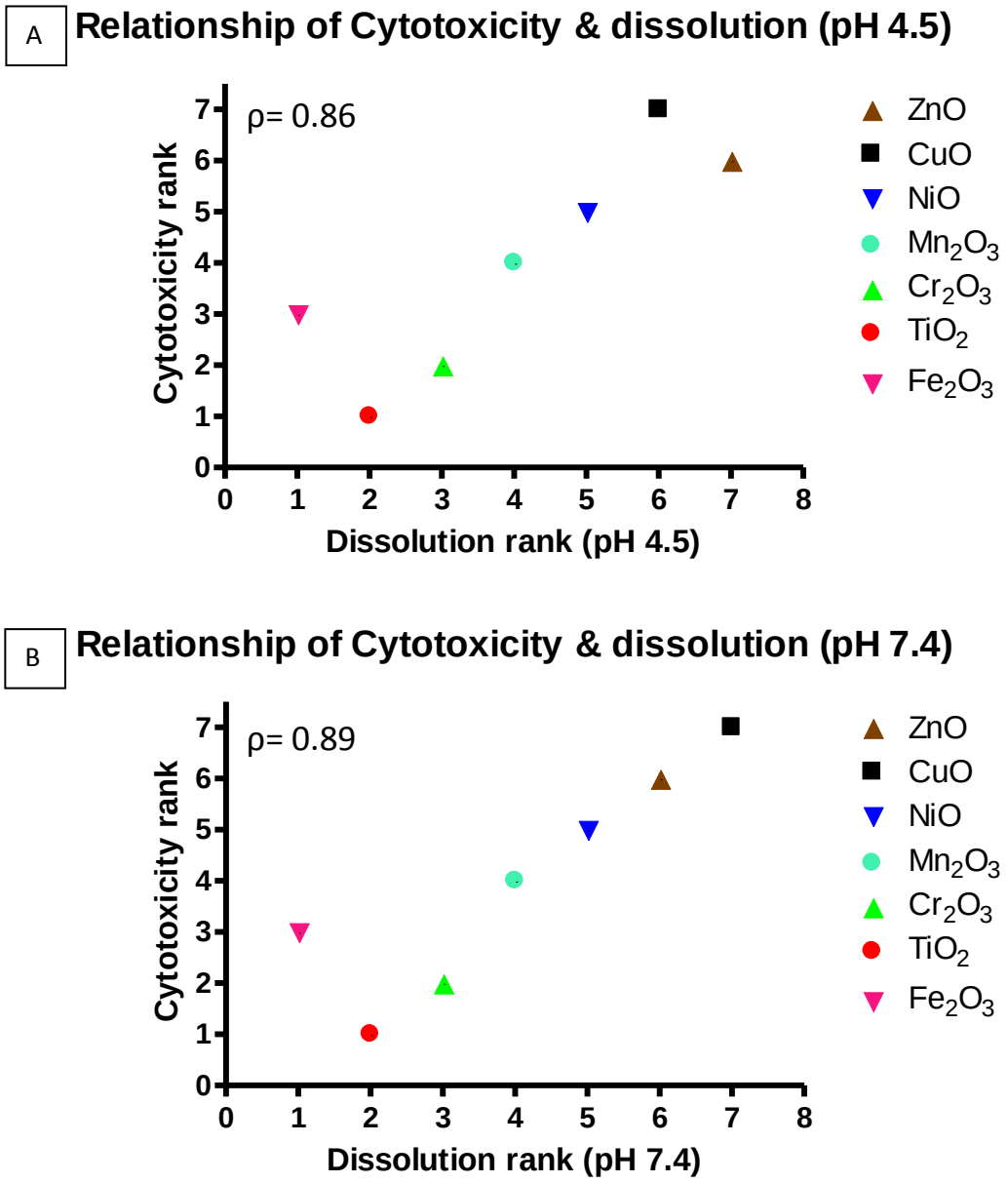

Figure 3.21: Relationship of cytotoxicity and dissolution (pH 4.5 and 7.4). A.) There is a strong correlation between cytotoxicity and dissolution at pH 4.5 (spearman's rank correlation coefficient, ρ = 0.86). B.) There is a strong correlation between cytotoxicity and dissolution at pH 7.4 (spearman's rank correlation coefficient, ρ = 0.89).

4. DISCUSSION

4.1 TRANSITION METAL OXIDE NANOPARTICLES CHARACTERIZATION

Characterization of nanoparticles was critical for the research when considering the different size, shape, and synthesis method could affect the cytotoxicity of nanoparticles. The preliminary TEM data of the transition metal oxide nanoparticles provided very important information such as particle size, morphology and appearance of the nanoparticles. Physical characteristics, such as morphology and size, provided by the company must be validated in the chance the values are misrepresented. TEM was employed to verify the characteristics of each nanoparticle (Table 3.1). The morphology of each nanoparticle was spherical in shape with the size coinciding with the information provided by supplier. The exception was TiO_2 which was needle shape instead of spherical, and Mn_2O_3 which was 82 ± 31 nm instead of 30-60 nm. According to the TEM images (Figure 3.1 to 3.7), the transition metal oxide nanoparticles were shown to form agglomerates which has been shown previously [24, 54, 55]. The decreasing size of particle was proposed to increase the effect on the cytotoxicity. It had been demonstrated that smaller nanoparticle with same composition had greater cytotoxicity. For instance, ZnO with APS of 27.16 nm caused 50 % cell viability at concentration as 15 μg/mL in A549 with 24 hr treatment (Figure 3.10 and 3.11). In other study, ZnO with APS of 52 nm caused 50% cell viability at concentration as 50 μg/mL [45]. This evidence indicated that a smaller size nanoparticle of same composition would cause higher cytotoxicity. Then, we were interested as to whether the different size of various composition nanoparticles would have the same trend. Based on the TEM data (Table 3.2), we demonstrated the correlation between cytotoxicity and APS. The ρ was -0.32 which indicates no increasing trend observed in the APS as cytotoxicity increased (Figure 3.8).

Nanoparticles with larger surface area per given mass correlated with increasing cytotoxicity by reactive atoms and molecules. SSA increases as the size of the particles

decreases and the increased SSA would be more reactive to intracellular compounds resulting in toxicity. However, according to the data in Table 3.2, we demonstrated the correlation between cytotoxicity and APS. The ρ was -0.32 which indicates there is no such trend that nanoparticles which had higher SSA would be more toxic (Figure 3.9). In conclusion, the particle size measurement and SSA measurement of the seven transition metal oxide nanoparticles indicated that both parameters were not significant factors in affecting the increasing cytotoxicity. Perhaps, there were some confounding factors which compromised or influenced the effect of APS and SSA such as point of zero charge, the number of available binding sites, and amount of released metal ion which are discussed in subsequent sections.

4.2 CYTOTOXICITY OF TRANSITION METAL OXIDES INCREASES AS ATOMIC NUMBER INCREASED

The specific nanoparticles were demonstrated to have different cytotoxicity on various cell lines [54]. A549, human alveolar adenocarcinoma cancer cell line, and BEAS-2B, bronchial epithelium derived cell line, were employed to clarify whether the cytotoxicity of nanoparticles was cell type specific. From our results (Figure 3.10 & 3.11), we concluded that the cytotoxicity of transition metal oxides was not cell line specific with the exception of ZnO which had 0-10 μg/mL cytotoxicity in BEAS-2B and 0-20 μg/mL cytotoxicity in A549. There was a steep relationship between concentrations (from 0 to 20 μg/mL) and reduction in cell viability (from 100% to 20%) treated with both BEAS-2B and A549 cells that were exposed to ZnO and CuO, respectively, for 24 hours. A curve relationship between concentrations (from 0 to 100 μg/mL) and reduction in cell viability (from 100% to 30%) was found in both cell lines exposed to NiO and Mn_2O_3 for 24 hr. The cytotoxicity data of Fe_2O_3, Cr_2O_3, and TiO_2 were shown to have only slight or no reduction in cell viability at 100 μg/mL. From this result, we defined three levels of cytotoxicity as none-to-minor, moderate, and steep. The ZnO and CuO were included in the steep cytotoxicity category, NiO and Mn_2O_3 were included in the moderate cytotoxicity category, and the none-to-minor cytotoxicity category included

Fe_2O_3, Cr_2O_3, and TiO_2. These three levels of cytotoxicity displayed the increasing trend, ordered with ascending atomic number of nanoparticle, as none-to-minor, moderate, and steep with the exception of Mn_2O_3. Although the Mn_2O_3 was supposed to be in a none-to-minor toxic group based on the increasing trend of the cytotoxicity, our observation defined it as moderate cytotoxicity. We demonstrated the correlation between cytotoxicity and atomic number. The ρ was 0.93 which indicates a strong correlation between cytotoxicity and atomic number **(**Figure 3.12**)**. This finding concluded that the cytotoxicity of transition metal oxides increased as their atomic number increased. The phenomenon aroused our curiosity as to whether there was a factor or multiple factors which could contribute to the increasing cytotoxicity of transition metal oxides.

4.3 POINT OF ZERO CHARGE ON SURFACE OF NANOPARTICLES INCREASED AS CYTOTOXICITY INCREASED

Point of zero charge was an important factor in the physicochemical properties. Evaluating the result from point of zero charge (Table 3.2 and Figure 3.13), PZC of transition metal oxides above 8.0 included NiO, CuO, ZnO, and Mn_2O_3 which were defined as mildly and severely cytotoxic, and the minor toxicity nanoparticles as TiO_2, Cr_2O_3, and Fe_2O_3 had PZC below 8.0. And there was an increasing value of PZC as atomic number of transition metal oxide rose. This observed trend matched the cytotoxicity of nanoparticles with the exception of Mn_2O_3 which showed the highest PZC of 8.8. The rationale for the deviation of Mn_2O_3 from periodic behavior with regard to PZC (and subsequent cytotoxicity) remains unclear. Moreover, the rationale for this observed trend can be understood by applying the principles underlying the Gouy-Chapman theory and considering the fact that attachment of intracellular material to these nanoparticulate surfaces were Coulombic in nature. When nanoparticles were exposed to an aqueous solution matrix below their PZC, the surface would get populated with an excess of hydronium ions and protons, making the nanoparticle surface positively charged which could attract and interact with negative charge intracellular molecules.

According to our result, the PZC of transition metal oxide nanoparticles were all above pH 7.4, or the cytosol pH value, with the exception of TiO_2 (PZC = 6.8). Once these nanoparticles were exposed to cytosol environment, the surface of the nanoparticles would become positively charge. Hence, negatively charged species such as phosphate groups of nucleic acid molecules (DNA and RNA) would be attracted to the nanoparticle surfaces. This interaction would cause further damage to cells. The fact that the PZC of TiO_2 is below pH = 7.4, and hence no Columbic attraction to intracellular material with an overall negative charge can occur, is one factor explaining its relative non-toxic character. Note that the cell viability is 100% in Figure 3.10 and 3.11, showing virtually no toxicity and taking into account the error bar. The PZC of Fe_2O_3 and Cr_2O_3 which was 8.0 and 7.8, respectively, may not attract enough intracellular material to cause any toxicity, or cell damage was remedied by other mechanisms which require further investigation. Interestingly, the most toxic of the nanoparticles, ZnO and CuO, which have the highest PZCs in the series, should be able to disrupt the cellular materials. We demonstrated the correlation between cytotoxicity and PZC. The ρ was 0.78 which indicated that the PZC increased as the cytotoxicity increased **(**Figure 3.14**)**. Our previous study reported that ZnO could cause DNA damage and alter the gene expressions [22, 51]. ZnO with 30 nm size and spherical shape treated on the A431 cell line for 6 hours at 5 and 0.8 μg/mL had caused DNA damage [80]. This rationale explained why nanoparticles of high PZC, above 8.0, were more toxic than materials that contain negatively charged groups. Cytotoxicity, in part, was governed by the resulting columbic attraction to cellular material based on a consequence of the PZC which seemed to increase with increasing atomic number of the transition metal within the oxide, with the exception of Mn_2O_3.

4.4 THE NUMBER OF AVAILABLE BINDING SITES OF TRANSITION METAL OXIDE INCREASED AS CYTOTOXICITY INCREASED

In addition to the observed trend in PZC, a periodicity in the number of available binding sites, as measured by XPS, was also correlated with toxicity trends. The number

of available binding sites on the surface of nanoparticles represented their chemical reactivity .The relative amount of adsorbed oxygen-to-metal oxide oxygen ratio, obtained from integrated XPS peak areas, was used as a means of quantifying the number of available binding sites to which intracellular material can interact via attachment. The greater the physisorbed oxygen-to-metal oxide oxygen ratio, the more adsorption sites are available for intracellular binding.

The adsorbates were predominantly adsorbed hydroxyl groups from H_2O; however, it would be noted that carbonates, CO and CO_2 from atmosphere, could be adsorb on the surface, and their BEs typically overlapped with the observed chemical shifts for adsorbed hydroxyls in the ~531 eV region. A trend of increasing adsorbed oxygen-to-metal oxide oxygen was observed for the series of metal oxides studied, with the exception of Cr_2O_3, which deviated in that it had a pronounced amount of adsorbed oxygen that was likely an artifact of CO_2 from solution exposure to atmosphere. CO_2 has a propensity to adsorb in a pronounced fashion onto Cr_2O_3. The relatively large XPS intensity at O 1 s BE at 531.2 eV (Figure 3.15) has also been reported to emanate from a mixed complex of $Cr_2O_3{\cdot}nH_2O{\cdot}xCO_2$ formed from adsorbed atmospheric CO_2 into aqueous solution [81]. The most toxic of nanoparticles analyzed in this series also have the highest adsorbed H_2O content; the vertical dashed line denotes the chemical oxidation state for adsorbed H_2O. ZnO and CuO have the highest PZCs and hence greatest degree of “protonation” via adsorption of hydronium ions (H_3O^+). We postulate that under aqueous solution physiological pH conditions, the metal oxide surface was populated by excess H_3O^+, in accordance with Gouy-Chapman theory. During adsorption, the adsorbate was electrically neutralized resulting in the observed enhanced intensity denoting chemisorbed H_2O at 532.9 eV on the CuO and ZnO surfaces. Adsorbed H_2O was not pronounced on the TiO_2, Mn_2O_3, Fe_2O_3 and NiO nanoparticulate surfaces. A lower intensity was observed for TiO_2 (Figure 3.15), which had the lowest PZC in the series (below that of physiological pH); however, it appears on the leading edge of the BE envelope indicative of adsorbed hydroxyls at 532 eV. We demonstrated the correlation between cytotoxicity and the number of available binding sites. The ρ was 0.71 which

indicates that the number of available binding sites increased as cytotoxicity increased (Figure 3.16). Cytotoxicity, in part, was governed by the available bind sites which seemed to increase with increasing atomic number of the transition metal within the oxide, with the exception of Cr_2O_3 and Mn_2O_3.

4.5 METAL DISSOLUTION OF TRANSITION METAL OXIDE CONTRIBUTES TO CYOTOXICITY

Our data indicate the transition metal oxides with higher cytotoxicity had more physicochemical reactivity. We were more interested in whether the transition metal oxide which might interact with excess hydronium in the aqueous condition would release the metal ion into the environment. During the dissolution experiments at pH 4.5, the nanoparticles of ZnO and CuO both disappeared in the solution within the first 3 hr, and the color of the solution turned from murky to transparent and light blue, respectively. The phenomenon above matched the result of high dissolution of ZnO and CuO (26% and 11%, respectively). The other nanoparticles, including NiO, Mn_2O_3, Fe_2O_3, Cr_2O_3, and TiO_2 would form a turbid solution, making it impossible to observe the reducing mass of nanoparticles.

ZnO nanoparticles tended to release more of the zinc ion under acidic conditions (pH 4.5) than under neutral conditions (pH 7.4). However, there was no significant linear relationship or increasing trend between dissolution and time (Figure 3.17). The similar pattern of dissolution appeared in CuO, NiO and Mn_2O_3 nanoparticles (Figure 3.18 to 3.20). In conclusion, the dissolution of ZnO, CuO, NiO and Mn_2O_3 nanoparticles showed no increasing trend nor significant linear relationship between various time points (6, 12, 18, and 24 hr) and two pH conditions (pH 4.5 and 7.4). This phenomenon could be explained by various uncontrollable parameters, such as agglomeration of the nanoparticles, adsorption by the beaker, and equilibrium between the nanoparticle and the free ion. For instance, we observed the nanoparticles would attach to the wall of beaker and formed a thick layer which may indicate adsorption. Regarding these issues, we are currently running more repeats of each transition metal oxide nanoparticles.

Overall, the dissolution of ZnO, CuO, NiO and Mn_2O_3 nanoparticles which were defined as severely and mildly cytotoxic tended to release more metal ions in an acidic environment (pH 4.5) than in a neutral environment (pH 7.4) (Table 3.3). Fe_2O_3, Cr_2O_3, and TiO_2 which were defined as the minorly cytotoxic had no significant dissolution (below 0.1%) at two different pH conditions (pH 4.5 and 7.4). Moreover, the result gave us an insight that the dissolution indeed had a relationship with cytotoxicity. We further demonstrated the correlation between cell viability and dissolution data at 24 hr, and there was a strong association at pH 4.5 and pH 7.4 (spearman's rank correlation coefficient, $\rho = 0.86$ and 0.89, respectively) (Figure 21). According to our result, we hypothesized that the transition metal oxide nanoparticles exposed to cells would be taken up, trapped and would release the metal ion in acidic environment (lysosome). The metal ion would be hardly released from nanoparticles which were exposed directly to the cytosol. When the nanoparticles triggered the cell death, it involved the interaction of the nanoparticles and intracellular molecules, as well as metal ion released from nanoparticles.

In this study, there was a strong correlation between dissolution of transition metal oxides and cytotoxicity at pH 4.5 and pH 7.4. Noteworthy, the dissolution rate of metal oxide was all below 1% at pH 7.4. At pH 4.5, the steeply cytotoxic group which included ZnO and CuO had the highest dissolution rates of 26% and 11%, respectively, and the moderately cytotoxic group which included NiO and Mn_2O_3 had the highest dissolution rates of 2% and 0.5%, respectively while the other metal oxides had dissolution rates below 0.1 %. This indicated the metal oxides present in cytosol would retain its integrity and do not interact with the hydronium while the metal oxides trapped in lysosome via endocytosis could release the metal ion. It became clear that the steep cytotoxicity of ZnO and CuO was mainly due to the released metal ion, and also accounted for PZC and the number of available binding sites. At the same time, the cytotoxicity of NiO and Mn_2O_3 mainly accounted for the PZC, the number of available binding sites, and the minor level of released metal ion.

5. CONCLUSION

The physicochemical characteristics of transition metal oxide such as morphology, APS, SSA, PZC, the number of available binding sites, and metal dissolution contributed to cytotoxicity were demonstrated in this study. We use the spearman's rank correlation coefficient to indicate whether there was any correlation between physicochemical properties and cytotoxicity. The cytotoxicity of transition metal oxide had strong correlation with atomic numbers. In other worlds, the cytotoxicity of transition metal oxide increased as atomic number went up. The results showed that APS and SSA had no correlation with the cytotoxicity of transition metal oxides. There was a strong correlation between PZC and cytotoxicity. The quantification of the number of available binding sites, done with XPS, also had a strong correlation with cytotoxicity. The metal dissolution of transition metal oxides was studied and showed a noteworthy result. At pH 7.4, the metal oxide barely released metal ions (dissolution below 0.1%). At pH 4.5, the ZnO and CuO which were steeply cytotoxic displaying the highest dissolution, the moderately cytotoxic NiO and Mn_2O_3 had dissolution around 2%, and minor dissolution was observed for TiO_2, Cr_2O_3, and Fe_2O_3 which were categorized as none-to-minor group. In summary, there was a strong correlation between metal dissolution and cytotoxicity.

Overall, the correlation between cytotoxicity and physicochemical properties of transition metal oxide nanoparticles such as PZC, the number of available binding sites, and dissolution were summarized in Table 5.1. Based on this information, we could conclude that the higher PZC of metal oxide nanoparticles was related with greater cytotoxicity. In the same way, higher number of available binding sites was associated with the greater cytotoxicity. Similarly, higher dissolution of metal oxide had correlated to greater cytotoxicity. Therefore, the observed trend in cytotoxicity is a consequence of multiple properties including PZC, available binding site, and dissolution. Overall, there is a periodicity in cytotoxicity across the 4^{th} period transition metal oxide nanoparticles

which are attributed to the physicochemical properties such as PZC, number of available surface binding sites and metal dissolution. This study presented the correlation between cytotoxicity and physicochemical characteristic which contributed to the cytotoxicity and gave an insight to develop strategies to remedy it. Future work will involve developing strategies to study and collect the effect of each physicochemical property to improve the safety of engineered nanoparticles.

Table 5.1**:** Summary of correlation between cytotoxicity and physicochemical characteristics

Relationship		Spearman's rank correlation coefficient (ρ)	Trend
Cytotoxicity	Atomic number	0.93	**Increasing**
	APS	-0.32	None
	SSA	-0.32	None
	PZC	0.78	**Increasing**
	The number of available binding sites	0.71	**Increasing**
	Dissolution (7.4)	0.89	**Increasing**
	Dissolution (4.5)	0.86	**Increasing**

REFERENCES

1. Council, N.R., *Small Wonders, Endless Frontiers: A Review of the National Nanotechnology Initiative.*, in *National Academy Press*2002: Washington, DC. p. 12.

2. USEPA, *ECONOMIC ANALYSIS OF THE PROPOSED CHANGE IN DATA REQUIREMENTS RULE FOR CONVENTIONAL PESTICIDES.* 2004.

3. Shinryo Yabe, M.Y., Shigeyoshi Momose, Kazuyuki Tahira, Sakae Yoshida , Ruixing Li , Shu Yin , Tsugio Sato, *Synthesis and UV-shielding properties of metal oxide doped ceria via soft solution chemical processes.* International Journal of Inorganic Materials, 2001. **3**: p. 1003-1008.

4. S. Roy, D.D., D. Chakravorty, and D. C. Agrawal, *Magnetic-properties of glass-metal nanocomposites prepared by the solgel route and hot pressing.* Journal of Applied Physics, 1993. **74**(7): p. 4746-4749.

5. Prinz, G.A., *Magnetoelectronics applications.* Journal of magnetism and magnetic materials, 1999. **200**: p. 57-68.

6. John K. Vassiliou, V.M., Michael W. Russell, Emmanuel P. Giannelis, R. D. McMichael et al., *Magnetic and optical-properties of gamma-Fe2O3 nanocrystals.* Journal of Applied Physics, 1993. **73**: p. 5109-5116.

7. S. S. Airapetyan, G.G.B., and A. G. Khachatryan, *Synthesis and Some Characteristics of Magnetic Matrices for Fixation of Biologically Active Substances.* Russian Journal of Applied Chemistry, 2000. **74**(3): p. 519-521.

8. S. Kobe, G.D., P.J. McGuiness, J. Strazisar, *The influence of the magnetic field on the crystallisation form of calcium carbonate and the testing of a magnetic water-treatment device.* Journal of Magnetism and Magnetic Materials, 2001. **236**: p. 71-76.

9. Akbarzadeh, A., M. Samiei, and S. Davaran, *Magnetic nanoparticles: preparation, physical properties, and applications in biomedicine.* Nanoscale Res Lett, 2012. **7**(1): p. 144.

10. Pedro Tartaj, M.d.P.M., Sabino Veintemillas-Verdaguer, Teresita Gonzalez-Carreno and Carlos J Serna, *The preparation of magnetic nanoparticles for applications in biomedicine.* JOURNAL OF PHYSICS D: APPLIED PHYSICS, 2003. **36**: p. 182-197.

11. Oberdorster, G., et al., *Acute pulmonary effects of ultrafine particles in rats and mice.* Res Rep Health Eff Inst, 2000(96): p. 5-74; disc 75-86.

12. Kevin E. Driscoll, D.L.C., Gary Hatch, Rogene Henderson, Gunter Oberdorster, Harry Salem and Richard B. Schlesinger, *Intratracheal Instillation as an Exposure Technique for the Evaluation of Respiratory Tract Toxicity: Uses and Limitations.* Toxicological Science, 2000. **55**: p. 24-35.

13. Brain, J.D., et al., *Pulmonary distribution of particles given by intratracheal instillation or by aerosol inhalation.* Environ Res, 1976. **11**(1): p. 13-33.

14. Li, X.Y., et al., *Short-term inflammatory responses following intratracheal instillation of fine and ultrafine carbon black in rats.* Inhal Toxicol, 1999. **11**(8): p. 709-31.

15. Wilson, M.R., et al., *Nanoparticle interactions with zinc and iron: implications for toxicology and inflammation.* Toxicol Appl Pharmacol, 2007. **225**(1): p. 80-9.

16. Martin R. Wilson, J.H.L., Ken Donaldson, Jill Sales, and Vicki Stone, *Interactions between Ultrafine Particles and Transition Metals in Vivo and in Vitro.* Toxicology and Applied Pharmacology, 2002. **184**: p. 172-179.

17. Dreher, K.L., *Health and environmental impact of nanotechnology: toxicological assessment of manufactured nanoparticles.* Toxicol Sci, 2004. **77**(1): p. 3-5.

18. Miller, R.J., et al., *Impacts of metal oxide nanoparticles on marine phytoplankton.* Environ Sci Technol, 2010. **44**(19): p. 7329-34.

19. Scown, T.M., R. van Aerle, and C.R. Tyler, *Review: Do engineered nanoparticles pose a significant threat to the aquatic environment?* Crit Rev Toxicol, 2010. **40**(7): p. 653-70.

20. Borm, P.J., et al., *The potential risks of nanomaterials: a review carried out for ECETOC.* Part Fibre Toxicol, 2006. **3**: p. 11.

21. Donaldson, K., et al., *Nanotoxicology.* Occup Environ Med, 2004. **61**(9): p. 727-8.

22. Huang, C.C., et al., *Oxidative stress, calcium homeostasis, and altered gene expression in human lung epithelial cells exposed to ZnO nanoparticles.* Toxicol In Vitro, 2010. **24**(1): p. 45-55.

23. Syed K Sohaebuddin, P.T.T., David Baker, John W Eaton, Liping Tang, *Nanomaterial cytotoxicity is composition, size, and cell type dependent.* Particle and fibre Toxicology, 2010. **7**(22): p. 17.

24. Karlsson, H.L., et al., *Copper oxide nanoparticles are highly toxic: a comparison between metal oxide nanoparticles and carbon nanotubes.* Chem Res Toxicol, 2008. **21**(9): p. 1726-32.

25. Bhattacharya, K., et al., *Titanium dioxide nanoparticles induce oxidative stress and DNA-adduct formation but not DNA-breakage in human lung cells.* Part Fibre Toxicol, 2009. **6**: p. 17.

26. Lin, S., et al., *High content screening in zebrafish speeds up hazard ranking of transition metal oxide nanoparticles.* ACS Nano, 2011. **5**(9): p. 7284-95.

27. Shaw, B.J. and R.D. Handy, *Physiological effects of nanoparticles on fish: a comparison of nanometals versus metal ions.* Environ Int, 2011. **37**(6): p. 1083-97.

28. Griffitt, R.J., et al., *Comparison of molecular and histological changes in zebrafish gills exposed to metallic nanoparticles.* Toxicol Sci, 2009. **107**(2): p. 404-15.

29. Khare, P., et al., *Adverse effects of TiO2 and ZnO nanoparticles in soil nematode, Caenorhabditis elegans.* J Biomed Nanotechnol, 2011. **7**(1): p. 116-7.

30. Fahmy, B. and S.A. Cormier, *Copper oxide nanoparticles induce oxidative stress and cytotoxicity in airway epithelial cells.* Toxicol In Vitro, 2009. **23**(7): p. 1365-71.

31. Kocbek, P., et al., *Toxicological aspects of long-term treatment of keratinocytes with ZnO and TiO2 nanoparticles.* Small, 2010. **6**(17): p. 1908-17.

32. Yue-Wern Huang, C.-h.W.a.R.S.A., *Toxicity of Transition Metal Oxide Nanoparticles: Recent Insights from in vitro Studies.* materials, 2012. **3**: p. 4842-4859.

33. Oberdorster, G., E. Oberdorster, and J. Oberdorster, *Nanotoxicology: an emerging discipline evolving from studies of ultrafine particles.* Environ Health Perspect, 2005. **113**(7): p. 823-39.

34. Oberdorster, G., et al., *Ultrafine particles as a potential environmental health hazard. Studies with model particles.* Chest, 1996. **109**(3 Suppl): p. 68S-69S.

35. Laskin, H.M.K.a.D.L., *Smaller is not always better: nanotechnology yields nanotoxicology.* Am J Physiol Lung Cell Mol Physiol, 2005. **289**: p. 696-697.

36. Nel, A., et al., *Toxic potential of materials at the nanolevel.* Science, 2006. **311**(5761): p. 622-7.

37. Mulder, W.J., et al., *Lipid-based nanoparticles for contrast-enhanced MRI and molecular imaging.* NMR Biomed, 2006. **19**(1): p. 142-64.

38. Lee, N., et al., *Water-Dispersible Ferrimagnetic Iron Oxide Nanocubes with Extremely High r(2) Relaxivity for Highly Sensitive in Vivo MRI of Tumors.* Nano Lett, 2012.

39. Osborne, E.A., et al., *Rapid microwave-assisted synthesis of dextran-coated iron oxide nanoparticles for magnetic resonance imaging.* Nanotechnology, 2012. **23**(21): p. 215602.

40. Hong, H., et al., *Cancer-targeted optical imaging with fluorescent zinc oxide nanowires.* Nano Lett, 2011. **11**(9): p. 3744-50.

41. Betty R. Liu, Y.-w.H., Jeffrey G. Winiarz, Huey-Jenn Chiang, Han-Jung Lee, *Intracellular delivery of quantum dots mediated by a histidine- and arginine-rich HR9 cell-penetrating peptide through the direct membrane translocation mechanism.* Biomaterials, 2001. **32**: p. 3520-3537.

42. Klostergaard, J. and C.E. Seeney, *Magnetic nanovectors for drug delivery.* Nanomedicine, 2012.

43. Krol, S., R. Ellis-Behnke, and P. Marchetti, *Nanomedicine for treatment of diabetes in an aging population: State-of-the-art and future developments.* Nanomedicine, 2012.

44. Parboosing, R., et al., *Nanotechnology and the Treatment of HIV Infection.* Viruses, 2012. **4**(4): p. 488-520.

45. Ahamed, M., et al., *ZnO nanorod-induced apoptosis in human alveolar adenocarcinoma cells via p53, survivin and bax/bcl-2 pathways: role of oxidative stress.* Nanomedicine, 2011. **7**(6): p. 904-13.

46. Horie, M., et al., *Evaluation of acute oxidative stress induced by NiO nanoparticles in vivo and in vitro.* J Occup Health, 2011. **53**(2): p. 64-74.

47. Tsukahara, T. and H. Haniu, *Cellular cytotoxic response induced by highly purified multi-wall carbon nanotube in human lung cells.* Mol Cell Biochem, 2011. **352**(1-2): p. 57-63.

48. Hussain, S., J.A. Vanoirbeek, and P.H. Hoet, *Interactions of nanomaterials with the immune system.* Wiley Interdiscip Rev Nanomed Nanobiotechnol, 2012. **4**(2): p. 169-83.

49. Inoue, K., *Promoting effects of nanoparticles/materials on sensitive lung inflammatory diseases.* Environ Health Prev Med, 2011. **16**(3): p. 139-43.

50. Inoue, K. and H. Takano, *Aggravating impact of nanoparticles on immune-mediated pulmonary inflammation.* ScientificWorldJournal, 2011. **11**: p. 382-90.

51. Weisheng Lin, Y.X., Chuan-Chin Huang, Yinfa Ma, Katie B. Shannon, Da-Ren Chen, Yue-Wern Huang, *Toxicity of nano- and micro-sized ZnO particles in human lung epithelial cells.* Journal Nanopart Res, 2009. **11**: p. 25-39.

52. Yang, H., et al., *Comparative study of cytotoxicity, oxidative stress and genotoxicity induced by four typical nanomaterials: the role of particle size, shape and composition.* J Appl Toxicol, 2009. **29**(1): p. 69-78.

53. Oberdorster, G., et al., *Role of the alveolar macrophage in lung injury: studies with ultrafine particles.* Environ Health Perspect, 1992. **97**: p. 193-9.

54. Hanley, C., et al., *The Influences of Cell Type and ZnO Nanoparticle Size on Immune Cell Cytotoxicity and Cytokine Induction.* Nanoscale Res Lett, 2009. **4**(12): p. 1409-20.

55. Karlsson, H.L., et al., *Size-dependent toxicity of metal oxide particles--a comparison between nano- and micrometer size.* Toxicol Lett, 2009. **188**(2): p. 112-8.

56. Chapman, D.L., *A contribution to the theory of electrocapillarity.* Philosophical Magazine, 1913. **25**: p. 475-481.

57. Gouy, G., *Electrocapillarity function.* Ann. Physique., 1917. **7**: p. 129-184.

58. Jaehyeon Park, J.R.R., *A Simple, Accurate Determination of Oxide PZC and the Strong Buffering Effect of Oxide Surfaces at Incipient Wetness.* Journal of Collod and Interface Science, 1995. **175**: p. 239-252.

59. JOLL, J.H.W., *X-ray Photoelectron Spectroscopy.* Accounts Chem. Res., 1970. **3**(17): p. 193-200.

60. Beck-Speier, I., et al., *Soluble iron modulates iron oxide particle-induced inflammatory responses via prostaglandin E(2)synthesis: In vitro and in vivo studies.* Part Fibre Toxicol, 2009. **6**: p. 34.

61. Xia, T., et al., *Comparison of the mechanism of toxicity of zinc oxide and cerium oxide nanoparticles based on dissolution and oxidative stress properties.* ACS Nano, 2008. **2**(10): p. 2121-34.

62. George, S., et al., *Use of a rapid cytotoxicity screening approach to engineer a safer zinc oxide nanoparticle through iron doping.* ACS Nano, 2010. **4**(1): p. 15-29.

63. Prahalad, A.K., et al., *Air pollution particles mediated oxidative DNA base damage in a cell free system and in human airway epithelial cells in relation to particulate metal content and bioreactivity.* Chem Res Toxicol, 2001. **14**(7): p. 879-87.

64. Mohd Javed Akhtar, M.A., Sudhir Kumar, Huma Siddiqui, Govil Patil, Mohd Ashquin, Iqbal Ahmad, *Nanotoxicity of pure silica mediated through oxidant generation rather than glutathione depletion in human lung epithelial cells.* Toxicology, 2010. **276**: p. 95-102.

65. Monks, A., et al., *Feasibility of a high-flux anticancer drug screen using a diverse panel of cultured human tumor cell lines.* J Natl Cancer Inst, 1991. **83**(11): p. 757-66.

66. Rubinstein, L.V., et al., *Comparison of in vitro anticancer-drug-screening data generated with a tetrazolium assay versus a protein assay against a diverse panel of human tumor cell lines.* J Natl Cancer Inst, 1990. **82**(13): p. 1113-8.

67. Wang, S., H. Yu, and J.K. Wickliffe, *Limitation of the MTT and XTT assays for measuring cell viability due to superoxide formation induced by nano-scale TiO2.* Toxicol In Vitro, 2011. **25**(8): p. 2147-51.

68. Stephen Brunauer, P.H.E., Edward Teller, *Adsorption of Gases in Multimolecular Layers.* J. Am. Chem. Soc., 1938. **60**(2): p. 309-319.

69. C. D. Wagner, D.A.Z., R. H. Raymond, *Use of the oxygen KLL Auger lines in identification of surface chemical states by electron spectroscopy for chemical analysis.* Anal. Chem., 1980. **58**(9): p. 1445-1451.

70. Masaoki Oku, K.H., *X-ray photoelectron spectroscopy of manganese—oxygen systems.* Journal of Electron Spectroscopy and Related Phenomena, 1975. **7**(5): p. 465-473.

71. J. Haber, J.S., L. Ungier, *X-ray photoelectron spectra of oxygen in oxides of Co, Ni, Fe and Zn.* Journal of Electron Spectroscopy and Related Phenomena, 1976. **9**(5): p. 459-467.

72. T., Y., *An X-ray photoelectron spectroscopic study of dioxime metal complexes.* Chem. Soc. Jpn., 1978. **51**: p. 3257-3260.

73. Joseph Chatt , C.M.E., Norman E. Hooper and G. Jeffery Leigh, *On the charge distribution in complexes.* Journal of the Chemical Society, Dalton Transactions, 1975(22): p. 2392-2401.

74. E.E Khawaja, M.A.S., M.A Khan, F.F Al-Adel, G.D Khattak, Z Hussain, *XPS, auger, electrical and optical studies of vanadium phosphate glasses doped with nickel oxide.* Journal of Non-Crystalline Solids, 1989. **10**(1): p. 33-43.

75. Allen, G.C.C., M. T.; Hooper, A. J.; Trucker, P. M., *X-ray photoelectron spectroscopy of chromium-oxygen systems.* J. Chem. Soc., 1973. **16**: p. 1675-1683.

76. Joseph C. Klein, C.P.L., David M. Hercules, and James F. Black *Decomposition of Copper Compounds in X-Ray Photoelectron Spectrometers.* Applied Spectroscopy, 1984. **38**(5): p. 729-734.

77. Chark, D.T.T., H. R., *Applications of ESCA to polymer chemistry. XVII. Systematic investigation of the core levels of simple homopolymers.* J. Polym. Sci. Polym. Chem. Ed., 1978. **16**: p. 791-820.

78. Chan-Cheng. Su, J.W.F., *Application of electron spectroscopy for chemical analysis to the study of ambidentate binding in sulfoxide complexes.* Inorganic Chemistry, 1974. **13**(7): p. 1734-1736.

79. V.I. Nefedov, M.N.F., I.S. Shaplygin, *Electronic structures of MRhO2, MRh2O4, RhMO4 and Rh2MO6 on the basis of X-ray spectroscopy and ESCA data.* Journal of Electron Spectroscopy and Related Phenomena, 1982. **26**(1): p. 65-78.

80. Sharma, V., et al., *DNA damaging potential of zinc oxide nanoparticles in human epidermal cells.* Toxicol Lett, 2009. **185**(3): p. 211-8.

81. Dale L. Perry, L.T., J.Ashley Taylor, *The galena/dichromate solution interaction and the nature of the resulting chromium(III) species.* Inorganica Chimica Acta, 1984. **85**(2): p. 57-60.

VITA

Chi-heng Wu was born on June 19th, 1983, in Hualien, Taiwan, R.O.C. He received his Bachelor of Science Degree in School of Medical Technology, Taipei Medical University in June, 2005. He served mandatory military service from 2005 to 2007. After the military sevice, he worked as research associate in National Taiwan University Hospital, from 2007-2009. In January 2010, he came to United States and enrolled in the Department of Biological Sciences pursing his Master Degree at the Missouri University of Science & Technology, and received his Master Degree in August, 2012.